Electronic Supplementary Material (ESI) for ChemComm.

Supporting Information for:

Late-stage ligand functionalization via the Staudinger reaction using phosphine-appended 2,2'-bipyridine

*Deeb Taher,[a,b] Jessica R. Wilson,[a] Grayson Ritch,[a] Matthias Zeller,[c] and Nathaniel K. Szymczak[a]**

[a] Department of Chemistry, University of Michigan, Ann Arbor, Michigan 48109, United States

[b] Department of Chemistry, The University of Jordan, Amman 11942, Jordan.

[c] H.C. Brown Laboratory, Department of Chemistry, Purdue University, West Lafayette, Indiana 44555, United States

Table of Contents:

	Experimental Procedures	4
Figure S1.	Infrared spectrum (KBr) of Ph_4P_2-bpyFeCl_2 (**1**).	8
Figure S2.	Infrared spectrum (KBr) of $\mathbf{2^{H}}$.	8
Figure S3.	Infrared spectrum (KBr) of $\mathbf{2^{tBu}}$.	9
Figure S4.	Infrared spectrum (KBr) of $\mathbf{2^{CF3}}$.	9
Figure S5.	Infrared spectrum (KBr) of $\mathbf{2^{2\text{-}OH}}$.	10
Figure S6.	Infrared spectrum (KBr) of $\mathbf{2^{3\text{-}OH}}$.	10
Figure S7.	Infrared spectrum (KBr) of $\mathbf{2^{2\text{-}BPin}}$.	11
Figure S8.	Infrared spectrum (KBr) of $\mathbf{2^{3\text{-}BPin}}$.	11
Figure S9.	^{1}H NMR spectrum ($CDCl_3$, 25 °C) of Ph_4P_2-bpyFeCl_2 (**1**).	12
Figure S10.	^{1}H NMR spectrum ($CDCl_3$, 25 °C) of $\mathbf{2^{H}}$.	13
Figure S11.	^{1}H NMR spectrum ($CDCl_3$, 25 °C) of $\mathbf{2^{tBu}}$.	14
Figure S12.	^{1}H NMR spectrum ($CDCl_3$, 25 °C) of $\mathbf{2^{CF3}}$.	15
Figure S13.	^{1}H NMR spectrum ($CDCl_3$, 25 °C) of $\mathbf{2^{2\text{-}OH}}$.	16
Figure S14.	^{1}H NMR spectrum ($CDCl_3$, 25 °C) of $\mathbf{2^{3\text{-}OH}}$.	17
Figure S15.	^{1}H NMR spectrum ($CDCl_3$, 25 °C) of $\mathbf{2^{2\text{-}BPin}}$.	18
Figure S16.	^{1}H NMR spectrum ($CDCl_3$, 25 °C) of $\mathbf{2^{2\text{-}BPin}}$.	19
Figure S17.	MALDI-TOF spectrum of Ph_4P_2-bpyFeCl_2 (**1**)	20
Figure S18.	MALDI-TOF spectrum of Ph_4P_2-bpyFeCl_2 (**1**).	21
Figure S19.	MALDI-TOF spectrum of $\mathbf{2^{H}}$.	22
Figure S20.	MALDI-TOF spectrum of $\mathbf{2^{tBu}}$.	23
Figure S21.	MALDI-TOF spectrum of $\mathbf{2^{CF3}}$.	24
Figure S22.	MALDI-TOF spectrum of $\mathbf{2^{2\text{-}OH}}$.	25
Figure S23.	MALDI-TOF spectrum of $\mathbf{2^{3\text{-}OH}}$.	26
Figure S24.	MALDI-TOF spectrum of $\mathbf{2^{2\text{-}BPin}}$.	27
Figure S25.	MALDI-TOF spectrum of $\mathbf{2^{3\text{-}BPin}}$.	28
Figure S26.	Electrochemical analysis of Ph_4P_2-bpyFeCl_2 (**1**) (4.4 mM) recorded in CH_2Cl_2 with 0.10 M $[Bu_4N][PF_6]$.	29
Figure S27.	Electrochemical analysis of Ph_4P_2-bpyFeCl_2 (**1**) (2.30 mM) dissolved in minimum CH_2Cl_2 and recorded in CH_3CN with 0.10 M $[Bu_4N][PF_6]$.	29
Figure S28.	Electrochemical analysis of Ph_4P_2-bpyFeCl_2 (**1**) (2.30 mM) dissolved in minimum CH_2Cl_2 and recorded in CH_3CN with 0.10 M $[Bu_4N][PF_6]$.	30
Figure S29.	Electrochemical analysis of Ph_4P_2-bpyFeCl_2 (**1**) (2.30 mM) dissolved in minimum CH_2Cl_2 and recorded in CH_3CN with 0.10 M $[Bu_4N][PF_6]$.	30
Figure S30.	Electrochemical analysis of $\mathbf{2^{H}}$ (1.13 mM) recorded in CH_2Cl_2 with 0.10 M $[Bu_4N][PF_6]$.	31
Figure S31.	Electrochemical analysis of $\mathbf{2^{H}}$ (2.83 mM) recorded in CH_3CN with 0.10 M $[Bu_4N][PF_6]$.	31
Figure S32.	Electrochemical analysis of 2tBu (1.40 mM) recorded in CH_2Cl_2 with 0.10 M $[Bu_4N][PF_6]$.	32
Figure S33.	Electrochemical analysis of $\mathbf{2^{tBu}}$ (1.90 mM) recorded in CH_3CN with 0.10 M $[Bu_4N][PF_6]$.	32
Figure S34.	Electrochemical analysis of $\mathbf{2^{CF3}}$ (2.48 mM) recorded in CH_2Cl_2 with 0.10 M $[Bu_4N][PF_6]$.	33

Figure S35.	Electrochemical analysis of $\mathbf{2^{CF3}}$ (1.47 mM) recorded in CH_3CN with 0.10 M $[Bu_4N][PF_6]$.	33
Figure S36.	Electrochemical analysis of $\mathbf{2^{2\text{-}OH}}$ (6.26 mM) recorded in CH_2Cl_2 with 0.10 M $[Bu_4N][PF_6]$.	34
Figure S37.	Electrochemical analysis of $\mathbf{2^{3\text{-}OH}}$ (7.39 mM) recorded in CH_2Cl_2 with 0.10 M $[Bu_4N][PF_6]$.	35
Figure S38.	Electrochemical analysis of $\mathbf{2^{2\text{-}BPin}}$ (5.44 mM) recorded in CH_2Cl_2 with 0.10 M $[Bu_4N][PF_6]$.	36
Figure S39.	Electrochemical analysis of $\mathbf{2^{3\text{-}BPin}}$ (6.86 mM) recorded in CH_2Cl_2 with 0.10 M $[Bu_4N][PF_6]$.	37
Figure S40.	Electrochemical analysis of $\mathbf{2^{x}}$ (x = H; ^{t}Bu, CF_3) recorded in CH_2Cl_2 with 0.10 M $[Bu_4N][PF_6]$.	38
Figure S41.	Electrochemical analysis of $\mathbf{2^{x}}$ (x = 2-OH; 3-OH; 2-BPin; 3-BPin) recorded in CH_2Cl_2 with 0.10 M $[Bu_4N][PF_6]$.	39
Figure 42.	Electronic absorption spectrum of Ph_4P_2-bpyFeCl_2 (**1**) recorded in CH_2Cl_2 at room temperature.	40
Figure 43.	Electronic absorption spectrum of $\mathbf{2^{x}}$ recorded in CH_2Cl_2 at room temperature.	41
Figure S44.	Plot of Hammett parameter (σp) vs energy for absorbance bands in UV-vis spectra of $\mathbf{2^{tBu}}$, $\mathbf{2^{H}}$, and $\mathbf{2^{CF3}}$.	42
Figure S45.	Molecular structure of Ph_4P_2-bpyFeCl_2 (**1**) with 50% probability ellipsoids. Hydrogen atoms are omitted for clarity.	43
Figure S46.	Molecular structure of $\mathbf{2^{H}}$ with 50% probability ellipsoids. Hydrogen atoms, solvents and PF_6^- are omitted for clarity.	44
Figure S47.	Molecular structure of $\mathbf{2^{H}}$.CH_3CN with 50% probability ellipsoids. Hydrogen atoms, solvents and PF_6^- are omitted for clarity.	45
Table S1.	Crystallographic parameters for Ph_4P_2-bpyFeCl_2 (**1**).	46
Table S2.	Crystallographic parameters for $\mathbf{2^{H}}$.	48
Table S3.	Crystallographic parameters for $\mathbf{2^{tBu}}$.	50
Table S4.	Crystallographic parameters for $\mathbf{2^{CF3}}$.	52
Table S5.	Crystallographic parameters for $\mathbf{2^{3\text{-}BPin}}$.	54
Figure S48.	Proposed solution structure of $\mathbf{2^{2\text{-}OH}}$.	56
	References	57

General Considerations. All air- and moisture-sensitive manipulations were performed using standard Schlenk techniques or in an inert atmosphere drybox with an atmosphere of purified nitrogen. The drybox was equipped with a cold well designed for freezing samples in liquid nitrogen as well as a −35 °C freezer for cooling samples and crystallizations. Solvents were purified using a Glass Contour solvent purification system through percolation through a Cu catalyst, molecular sieves, and alumina. Solvents were then stored over sodium and/or sieves. Chloroform-d were purchased from Cambridge Isotope Laboratories. Chloroform-d was distilled from CaH_2 and stored over molecular sieves. 2,6-Dibromopyridine, n-butyllithium, aniline, 4-tert-butylaniline, 4-(trifluoromethyl)aniline, 2-aminophenol, 3-aminophenol, 2-(4,4,5,5-Tetramethyl-1,3,2-dioxaborolan-2-yl)aniline, 3-(4,4,5,5-tetramethyl-1,3,2-dioxaborolan-2-yl)aniline, $FeCl_2$, chlorodiphenylphosphine, and sodium hexafluorophosphate were purchased from commercial vendors and used as received. Azidobenzene,[1] 1-azido-4-(tert-butyl)benzene, [2] 1-azido-4-(trifluoromethyl)benzene,1-azido-4-(tert-butyl)benzene,[3] 2-azidophenol,[4] 3-azidophenol, [5] 2-(2-azidophenyl)-4,4,5,5-tetramethyl-1,3,2-dioxaborolane, [6] 3-(2-azidophenyl)-4,4,5,5-tetramethyl-1,3,2-dioxaborolane,[7] $bpyBr_2$[8] and 6,6'-bis(diphenylphosphanyl)-2,2'-bipyridine [9] were synthesized according to literature procedures.

NMR spectra were recorded on Varian Vnmrs 700 or Varian MR400 spectrometers. ^{1}H, chemical shifts are reported in parts per million (ppm) relative to tetramethylsilane and referenced internally to the residual solvent peak. Multiplicities are reported as follows: The spectra for paramagnetic molecules were obtained by using an acquisition time of 0.5 s, thus the peak widths reported have an error of ±2 Hz. Infrared spectra were recorded using a Nicolet iS10 FTIR spectrometer. Samples were diluted into dry KBr and recorded as pellets. Electronic absorption spectra were recorded at ambient temperature in sealed 1 cm quartz cuvettes with a Varian Cary-50 spectrophotometer. MALDI-TOF data were collected on a Bruker AutoFlex Speed with samples prepared under inert atmosphere in an anthracene matrix.

Single crystals of **1**, $\mathbf{2^{H}}$, $\mathbf{2^{tBu}}$ and $\mathbf{2^{CF3}}$ suitable for X-ray diffraction were coated with poly(isobutylene) oil in a drybox and mounted on a Rigaku AFC10K Saturn 944+ CCD-based X-ray diffractometer equipped with a low temperature device and Micromax-007HF Cu-target microfocus rotating anode (λ = 1.54187 Å). The data were collected using CrystalClear 2.011[10] and processed using CrysAlis PRO 1.171.38.41.[10] Empirical absorption correction was applied using spherical harmonics, as implemented in the SCALE3 ABSPACK[11] scaling algorithm. Single crystals of $\mathbf{2^{3\text{-}BPin}}$ suitable for X-ray diffraction, were coated with poly(isobutylene) oil in a drybox and quickly transferred to the goniometer head of a Bruker AXS D8 Quest diffractometer with a fixed chi angle, a sealed tube fine focus X-ray tube, single crystal curved graphite incident beam monochromator and a PhotonII CPAD area detector. Examination and data collection were performed with Mo Kα radiation (λ = 0.71073 Å). The data were collected, reflections were indexed and processed, and the files scaled and corrected for absorption using SADABS 2016/2[12]. For all samples, the space groups were assigned and the structures were solved by direct methods using XPREP within the SHELXTL suite of programs[13] and refined by full matrix least squares against F^2 with all reflections using Shelxl2018[14] using the graphical interface Shelxle.[15] If not specified otherwise, H atoms attached to carbon atoms were positioned geometrically and constrained to ride on their parent atoms, with carbon hydrogen bond distances of 0.95 Å for and aromatic C-H, 1.00, 0.99 and 0.98 Å for aliphatic C-H, CH_2, and CH_3 moieties, respectively. Methyl H atoms were allowed to rotate but not to tip to best fit the experimental electron density. U_{iso}(H) values were set to a multiple of U_{eq}(C) with 1.5 for CH_3, and 1.2 for CH_2, and C-H units, respectively. Additional data collection and refinement details, including description of disorder (where

present) can be found with the individual structure descriptions, below. Complete crystallographic data, in CIF format, have been deposited with the Cambridge Crystallographic Data Centre. CCDC 2070170-2070174 contain the supplementary crystallographic data for this paper. These data can be obtained free of charge from The Cambridge Crystallographic Data Centre via www.ccdc.cam.ac.uk/data_request/cif.

Experimental Procedures

Synthesis of Ph_4P_2-bpyFeCl_2 (1). 6,6'-bis(diphenylphosphanyl)-2,2'-bipyridine (500 mg, 0.953 mmol) and iron (II) chloride (121 mg, 0.953 mmol) was suspended in 20 mL of THF. After approximately 30 minutes and new orange precipitate begins to form. The suspension was allowed to stir overnight before the orange solid was isolated. The resulting orange material was washed with 20 mL of diethyl ether and dried to afford orange powder (520 mg yield, 0.800 mmol, 84%). A crystal of **1** suitable for X-ray diffraction was grown by vapor diffusion of diethyl ether into a concentrated dichloromethane-THF solution of **1** at room temperature. ^{1}H-NMR (400MHz, CD_2Cl_2, 25 °C): δ74.62, 52.16, 4.60, 4.37, -3.80, -17.18. μ_{eff} ($CDCl_3$, 25 °C) = 5.57±0.4. MALDI-TOF of $C_{34}H_{25}Cl_2FeN_2P_2$ (M- H): Calc. Calc.649.018; Found 649.264. UV-Vis (DCM, ambient temperature; λ_{max}, molar absorptivity): 511 nm, 113.5 $M^{-1}cm^{-1}$; 304 nm, 15853 $M^{-1}cm^{-1}$. Anal. calcd. for $C_{34}H_{26}Cl_2FeN_2P_2$ (650.03 g/mol): C, 62.70; H, 4.02; N, 4.30. Found C, 62.34; H, 4.35; N, 4.23 %. $E_{1/2}$ (0.1M $TBAPF_6$ in DCM, vs Fc/Fc^+): 373 mV.

Synthesis of 2^H. Ph_4P_2-bpyFeCl_2 (100 mg, 0.154 mmol) and sodium hexafluorophosphate (25.8 mg, 0.077 mmol) were suspended in 15 mL of THF. Azidobenzene (36.6 mg, 0.308 mmol) dissolved in 5 mL of THF was added all at once to the suspension. Within 30 minutes a new cloudy blue precipitate had begun to form. The suspension was allowed to stir overnight at room temperature. Volatiles were removed via vacuum and the resulting solid was extracted with 15 mL DCM. The DCM was removed to yield a dark blue solid (139 mg yield, 0.147 mmol, 95%). A crystal of $\mathbf{2^H}$ suitable for X-ray diffraction was grown by vapor diffusion of diethyl ether into a concentrated acetonitrile solution of $\mathbf{2^H}$ at room temperature. ^{1}H-NMR (400MHz, $CDCl_3$, 25 °C): δ79.96, 69.55, 58.87, 52.85, 26.42, 24.66, 20.98, 15.29, 13.74, 13.37, 11.65, 9.74, 9.41, 9.25, 5.39, 4.61, -4.60, -5.33, -6.40, -7.77, -27.87, -36.04. μ_{eff} ($CDCl_3$, 25 °C) = 4.93±0.4. MALDI-TOF of $C_{46}H_{36}ClFeN_4P_2$ (M- PF_6): Calc. 797.148; Found 797.576. UV-Vis (DCM, ambient temperature; λ_{max}, molar absorptivity): 615 nm, 1791 $M^{-1}cm^{-1}$; 466 nm, 1753 $M^{-1}cm^{-1}$. The obtained powders were used for combustion analyses. Anal. calcd. for $C_{46}H_{36}ClF_6FeN_4P_3$ (943.03 g/mol): C, 58.59; H, 3.85; N, 5.94. Found C, 58.82; H, 3.90; N, 6.36 %. $E_{1/2}$ (0.1M $TBAPF_6$ in DCM, vs Fc/Fc^+): 30 mV.

Synthesis of 2^{tBu}. Ph_4P_2-bpyFeCl_2 (100 mg, 0.154 mmol) and sodium hexafluorophosphate (25.8 mg, 0.077 mmol) were suspended in 15 mL of THF. 1-Azido-4-(tert-butyl)benzene (54 mg, 0.308 mmol) dissolved in 5 mL of THF was added all at once to the suspension. Within 30 minutes a new cloudy blue precipitate had begun to form. The suspension was allowed to stir overnight at room temperature. Volatiles were removed via vacuum and the resulting solid was extracted with 15 mL DCM. The DCM was removed to yield a dark blue solid (150 mg yield, 0.142 mmol, 92%). Crystals of $\mathbf{2^{tBu}}$ suitable for X-ray diffraction were grown by vapor diffusion of diethyl ether into a concentrated acetonitrile solution of $\mathbf{2^{tBu}}$ at room temperature. ^{1}H-NMR (400MHz, $CDCl_3$, 25 °C): δ80.42, 51.52, 25.42, 22.70, 15.38, 15.04, 12.73, 11.69, 9.74, 9.40, 5.00, 1.32, 0.202, -1.15, -1.43, -33.38. μ_{eff} ($CDCl_3$, 25 °C) = 4.96±0.4. MALDI-TOF of

$C_{54}H_{52}ClFeN_4P_2$ (M- PF_6): Calc. 909.659; Found 909.271. UV-Vis (DCM, ambient temperature; λ_{max}, molar absorptivity): 630 nm, 1787 $M^{-1}cm^{-1}$; 478 nm, 1431 $M^{-1}cm^{-1}$. The crystals were used for combustion analyses. Anal. calcd. for $C_{54}H_{52}ClF_6FeN_4P_3.1.279Et_2O.0.666CH_3CN$: solvate from X-ray structure (1177.39 g/mol): C, 61.67; H, 5.72; N, 5.55. Found C, 57.51; H, 4.43; N, 5.51 %. $E_{1/2}$ (0.1M $TBAPF_6$ in DCM, vs Fc/Fc^+): 184 mV.

Synthesis of 2^{CF3}. Ph_4P_2-bpyFeCl_2 (100 mg, 0.154 mmol) and sodium hexafluorophosphate (25.8 mg, 0.077 mmol) were suspended in 15 mL of THF. 1-Azido-4-(trifluoromethyl)benzene (57.6 mg, 0.308 mmol) dissolved in 5 mL of THF was added all at once to the suspension. Within 30 minutes a new cloudy blue precipitate had begun to form. The suspension was allowed to stir overnight at room temperature. Volatiles were removed via vacuum and the resulting solid was extracted with 15 mL DCM. The DCM was removed to yield a dark blue solid (138 mg yield, 0.128 mmol, 83%).%). A crystal of $\mathbf{2^{CF3}}$ suitable for X-ray diffraction was grown by vapor diffusion of diethyl ether into a concentrated acetonitrile solution of $\mathbf{2^{CF3}}$ at room temperature. ^{1}H-NMR (400MHz, CH_2Cl_2, 25 °C): 79.57, 56.64, 25.47, 14.90, 14.38, 12.96, 9.80, 1.25, 1.14, -31.86. μ_{eff} (CH_2Cl_2, 25 °C) = 4.92±0.4. MALDI-TOF of $C_{48}H_{34}ClF_6FeN_4P_2$ (M- PF_6): Calc. 933.120; Found 933.502. UV-Vis (DCM, ambient temperature; λ_{max}, molar absorptivity): 593 nm, 2945 $M^{-1}cm^{-1}$; 454 nm, 3232 $M^{-1}cm^{-1}$. The isolated crystals were used for combustion analyses. Anal. calcd. for $C_{48}H_{34}ClF_{12}FeN_4P_3.1.155Et_2O.$ 0.734CH_3CN: solvate from X-ray structure (1194.77 g/mol): C, 54.37; H, 4.03; N, 5.55. Found C, 56.05; H, 3.31; N, 4.80 %. $E_{1/2}$ (0.1M $TBAPF_6$ in DCM, vs Fc/Fc^+): 160 mV.

Synthesis of $2^{2\text{-}OH}$. Ph_4P_2-bpyFeCl_2 (100 mg, 0.154 mmol) and sodium hexafluorophosphate (25.8 mg, 0.077 mmol) were suspended in 15 mL of THF. 2-azidophenol (41.6 mg, 0.308 mmol) dissolved in 5 mL of THF was added all at once to the suspension. Within 30 minutes a new cloudy blue precipitate had begun to form. The suspension was allowed to stir overnight at room temperature. Volatiles were removed via vacuum and the resulting solid was extracted with 15 mL DCM. The DCM was removed to yield a dark blue solid (135 mg yield, 0.138 mmol, 90%).^{1}H-NMR (400MHz, $CDCl_3$, 25 °C): δ15.20, 7.75, 6.77, 0.30, 0.14, -1.89. MALDI-TOF of $C_{46f}H_{35}FeN_4O_2P_2$ (M- (HCL +PF_6)): Calc. 793.158; Found 792.405. UV-Vis (DCM, ambient temperature; λ_{max}, molar absorptivity): 690 nm, 1306 $M^{-1}cm^{-1}$. The obtained powders were used for combustion analyses. Anal. calcd. for $C_{46}H_{36}ClF_6FeN_4O_2P_3$ (974.10 g/mol): C, 56.67; H, 3.72; N, 5.75. Found C, 57.08; H, 3.74; N, 5.51 %. $E_{1/2}$ (0.1M $TBAPF_6$ in DCM, vs Fc/Fc^+): –465 mV

Synthesis of $2^{3\text{-}OH}$. Ph_4P_2-bpyFeCl_2 (100 mg, 0.154 mmol) and sodium hexafluorophosphate (25.8 mg, 0.077 mmol) were suspended in 15 mL of THF. 3-azidophenol (41.6 mg, 0.308 mmol) dissolved in 5 mL of THF was added all at once to the suspension. Within 30 minutes a new cloudy blue precipitate had begun to form. The suspension was allowed to stir overnight at room temperature. Volatiles were removed via vacuum and the resulting solid was extracted with 15 mL DCM. The DCM was removed to yield a dark blue solid (112 mg yield, 0.115 mmol, 75%).^{1}H-NMR (400MHz, $CDCl_3$, 25 °C): δ80.15, 53.74, 26.88, 21.30, 15.24, 13.78, 13.25, 9.89, 4.72, 3.72, 3.48, 1.22, 0.88, -1.84, -1.96, -4.83, -26.24, -27.06. MALDI-TOF of $C_{46}H_{35}FeN_4O_2P_2$ (M- PF_6): Calc. 829.135; Found 829.414. UV-Vis (DCM, ambient temperature; λ_{max}, molar absorptivity): 610 nm, 2273 $M^{-1}cm^{-1}$. The obtained powders were used for combustion analyses. Anal. calcd. for $C_{46}H_{36}ClF_6FeN_4O_2P_3$ (974.10 g/mol): C, 56.67; H, 3.72; N, 5.75. Found C, 56.00; H, 4.63; N, 5.91 %. $E_{1/2}$ (0.1M $TBAPF_6$ in DCM, vs Fc/Fc^+): 25 mV.

Synthesis of $2^{2\text{-BPin}}$. Ph_4P_2-bpyFeCl_2 (100 mg, 0.154 mmol) and sodium hexafluorophosphate (25.8 mg, 0.077 mmol) were suspended in 15 mL of THF. 2-(2-azidophenyl)-4,4,5,5-tetramethyl-1,3,2-dioxaborolane (75.5 mg, 0.308 mmol) dissolved in 5 mL of THF was added all at once to the suspension. Within 30 minutes a new cloudy blue precipitate had begun to form. The suspension was allowed to stir overnight at room temperature. Volatiles were removed via vacuum and the resulting solid was extracted with 15 mL DCM. The DCM was removed to yield a dark blue solid (152 mg yield, 0.127 mmol, 83%).^{1}H-NMR (400MHz, $CDCl_3$, 25 ^{o}C): δ79.87, 73.26, 24.95, 18.42, 16.67, 14.31, 13.88, 13.36, 12.95, 9.73, 8.43, 7.96, 7.81, 7.73, 6.07, 5.94, 4.05, 1.97, 1.94, 1.74, 1.38, 1.31, 1.27, 1.10, 0.19, -1.27, -3.14 -17.99. MALDI-TOF of $C_{58}H_{58}B_2ClFeN_4O_2P_2$ (M- PF_6): Calc. 1049.316; Found 1049.542. UV-Vis (DCM, ambient temperature; λ_{max}, molar absorptivity): 607 nm, 1123 $M^{-1}cm^{-1}$; 458 nm, 1558 $M^{-1}cm^{-1}$. The obtained powders were used for combustion analyses. Anal. calcd. for $C_{58}H_{58}B_2ClF_6FeN_4O_2P_3$ (1194.95 g/mol): C, 58.30; H, 4.89; N, 4.69. Found C, 58.40; H, 4.79; N, 5.36 %. $E_{1/2}$ (0.1M $TBAPF_6$ in DCM, vs Fc/Fc^+): 178 mV.

Synthesis of $2^{3\text{-BPin}}$. Ph_4P_2-bpyFeCl_2 (100 mg, 0.154 mmol) and sodium hexafluorophosphate (25.8 mg, 0.077 mmol) were suspended in 15 mL of THF. 3-(2-azidophenyl)-4,4,5,5-tetramethyl-1,3,2-dioxaborolane (75.5 mg, 0.308 mmol) dissolved in 5 L of THF was added all at once to the suspension. Within 30 minutes a new cloudy blue precipitate had begun to form. The suspension was allowed to stir overnight at room temperature. Volatiles were removed via vacuum and the resulting solid was extracted with 15 mL DCM. The DCM was removed to yield a dark blue solid (165 mg yield, 0.138 mmol, 90%). A crystal of **$2^{3\text{-BPin}}$** suitable for X-ray diffraction was grown by vapor diffusion of diethyl ether into a concentrated acetonitrile solution of **$2^{3\text{-BPin}}$** at room temperature. ^{1}H-NMR (400MHz, $CDCl_3$, 25 ^{o}C): δ79.37, 47.54, 25.97, 22.34, 14.96, 13.23, 9.67, 4.55, 1.36, -0.50, -0.55, -26.51, -35.32. MALDI-TOF of $C_{58}H_{58}B_2ClFeN_4O_2P_2$ (M- PF_6): Calc. 1049.316; Found 1049.632. UV-Vis (DCM, ambient temperature; λ_{max}, molar absorptivity): 628 nm, 1255 $M^{-1}cm^{-1}$; 474 nm, 1127 $M^{-1}cm^{-1}$. The obtained powders were used for combustion analyses. Anal. calcd. for $C_{58}H_{58}B_2ClF_6FeN_4O_2P_3$ (1194.95 g/mol): C, 58.30; H, 4.89; N, 4.69. Found C, 58.96; H, 4.90; N, 4.77 %. $E_{1/2}$ (0.1M $TBAPF_6$ in DCM, vs Fc/Fc^+): 239 mV.

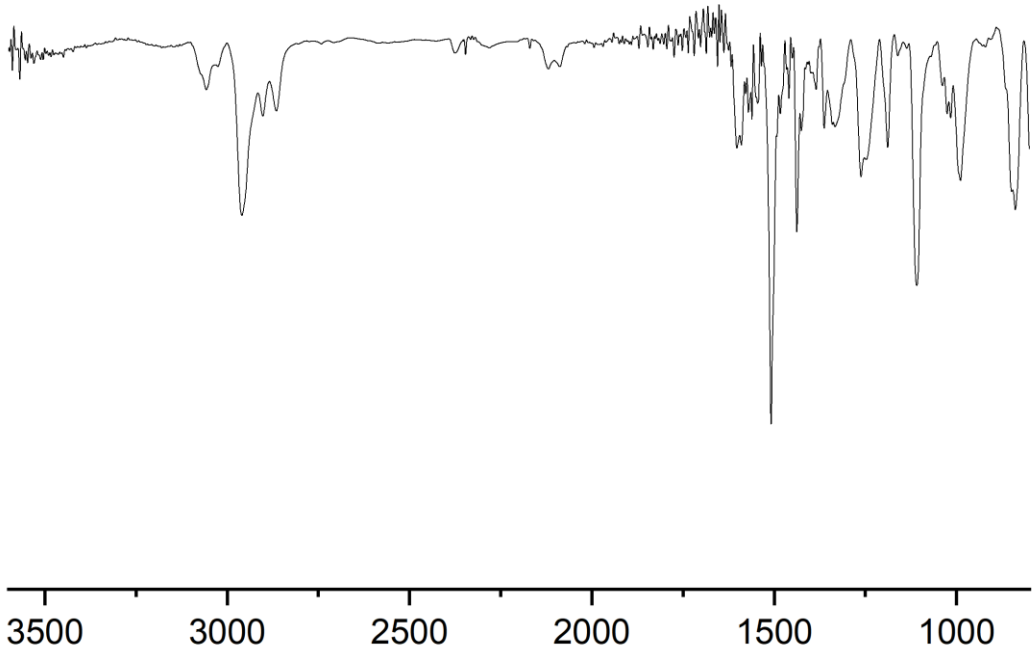

Figure S1. Infrared spectrum (KBr) of **Ph_4P_2-bpyFeCl_2 (1).**

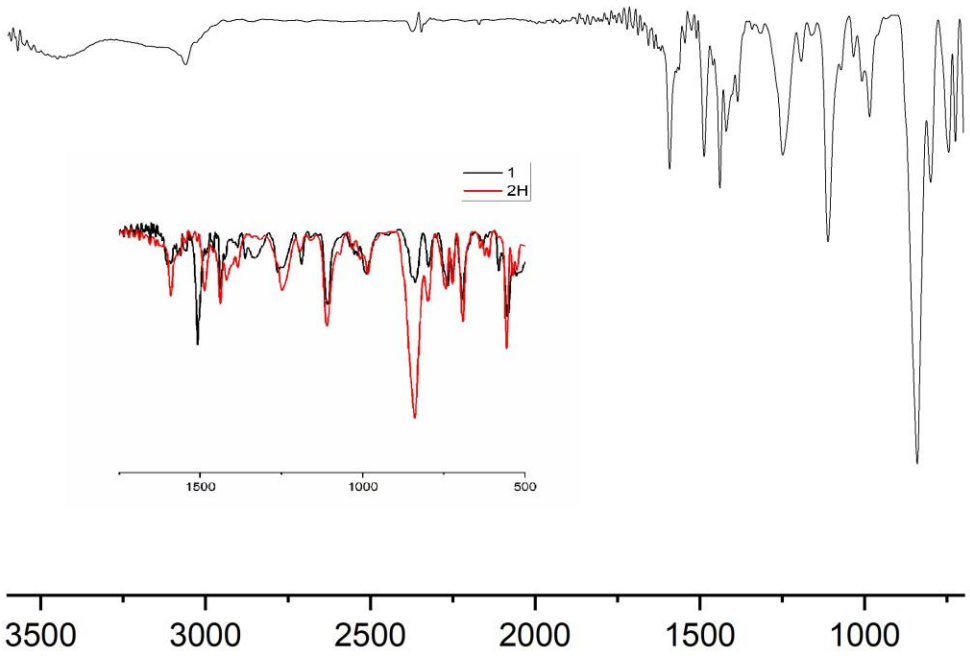

Figure S2. Infrared spectrum (KBr) of **2^H**.

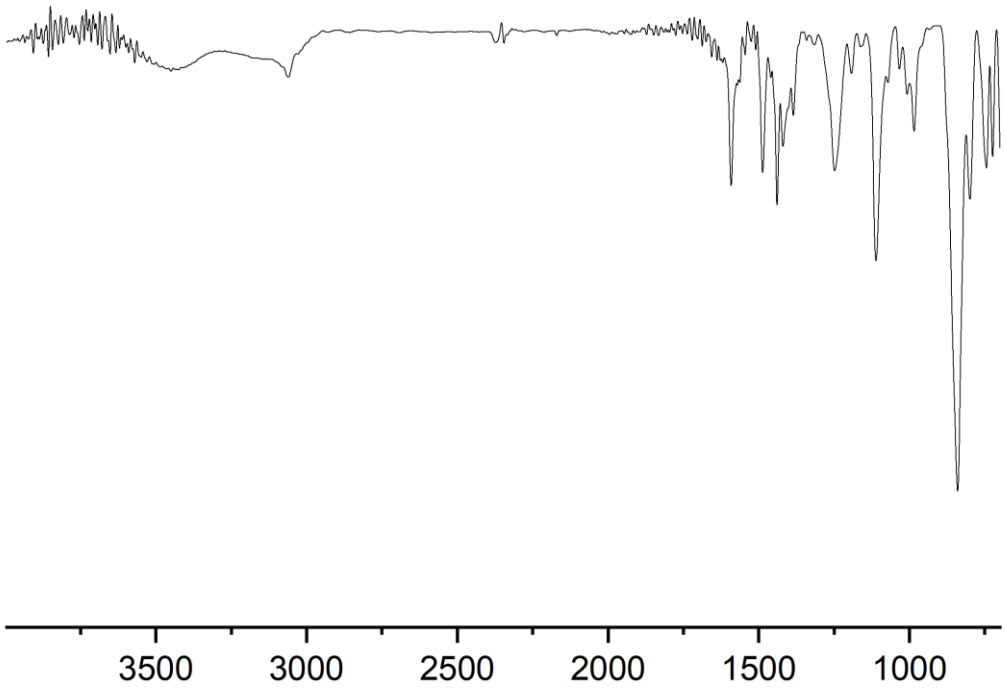

Figure S3. Infrared spectrum (KBr) of **2**^{tBu}.

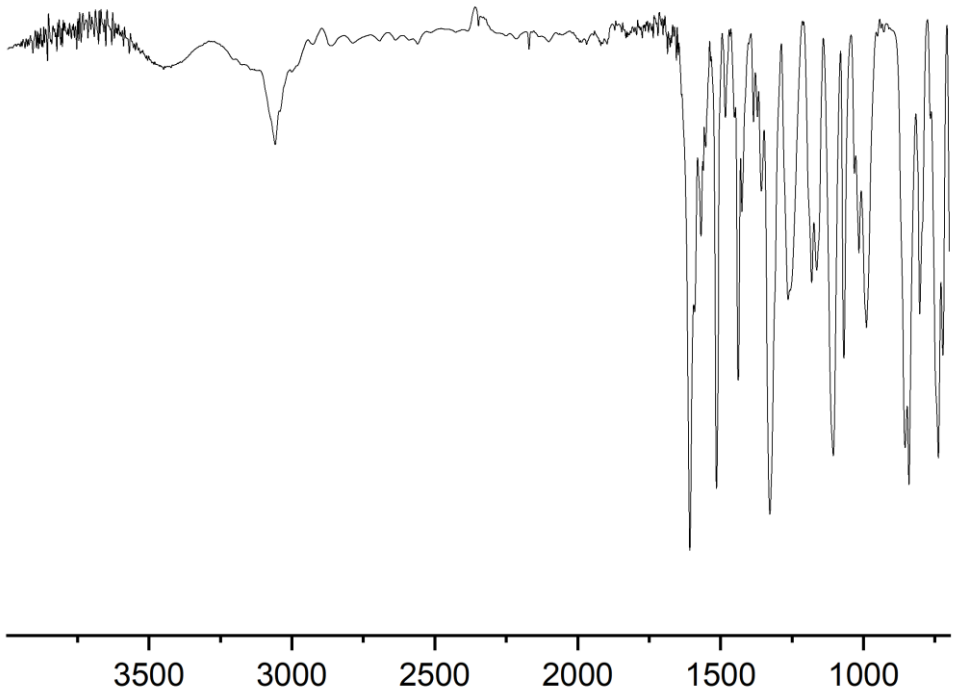

Figure S4. Infrared spectrum (KBr) of **2**^{CF3}.

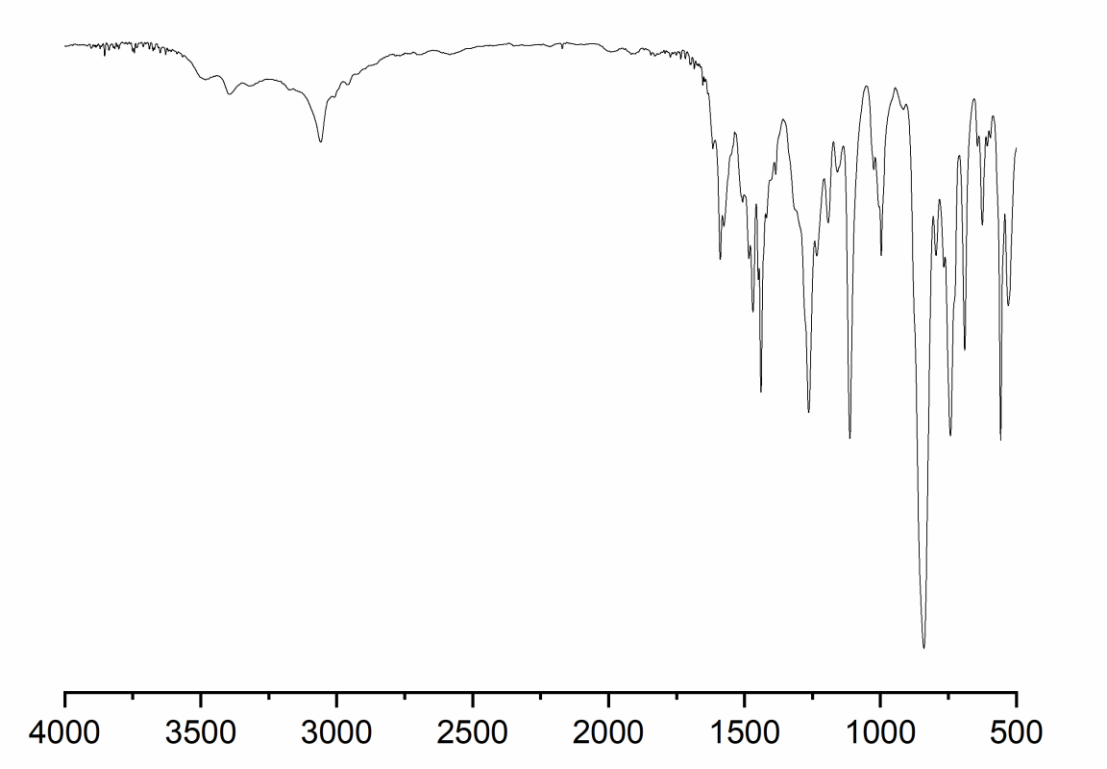

Figure S5. Infrared spectrum (KBr) of $\mathbf{2}^{\mathbf{2\text{-}OH}}$.

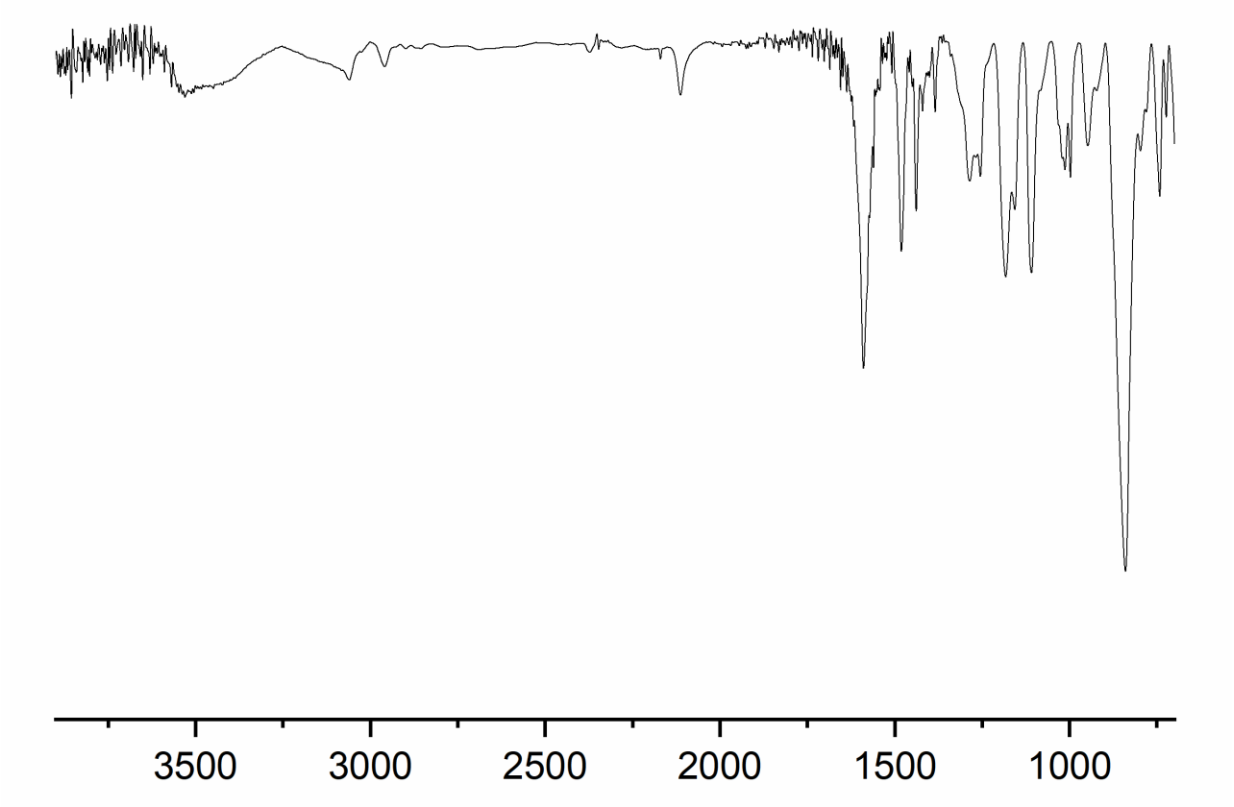

Figure S6. Infrared spectrum (KBr) of $\mathbf{2}^{\mathbf{3\text{-}OH}}$.

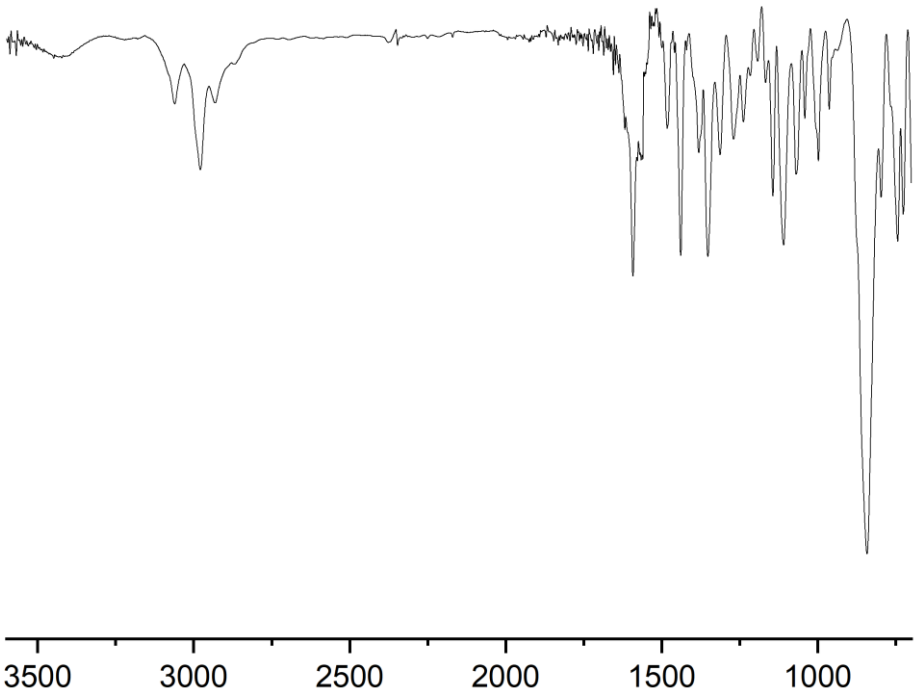

Figure S7. Infrared spectrum (KBr) of **2**$^{3\text{-BPin}}$.

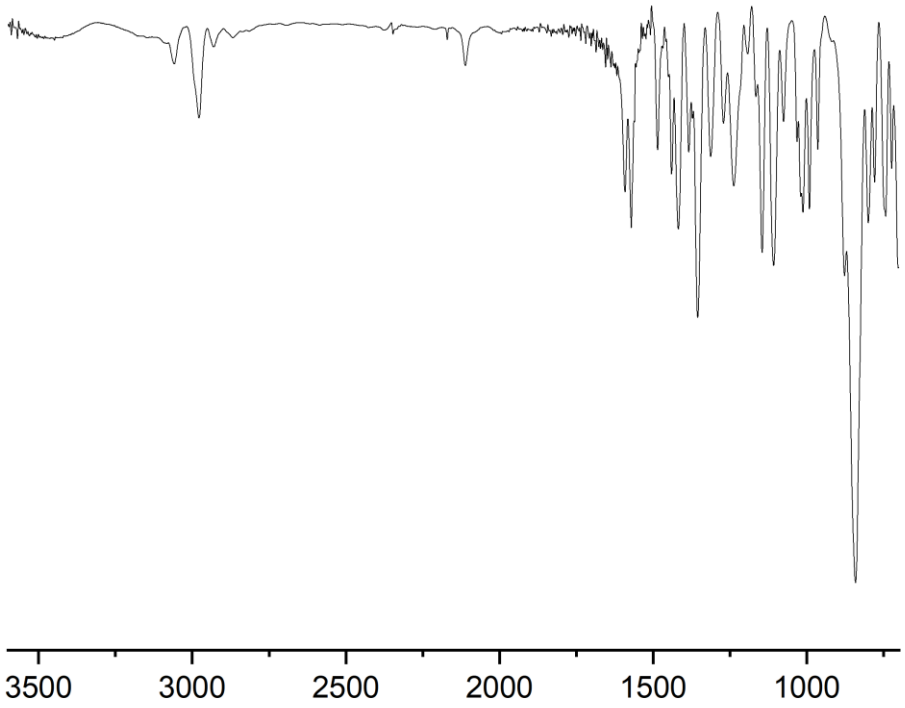

Figure S8. Infrared spectrum (KBr) of **2**$^{3\text{-BPin}}$.

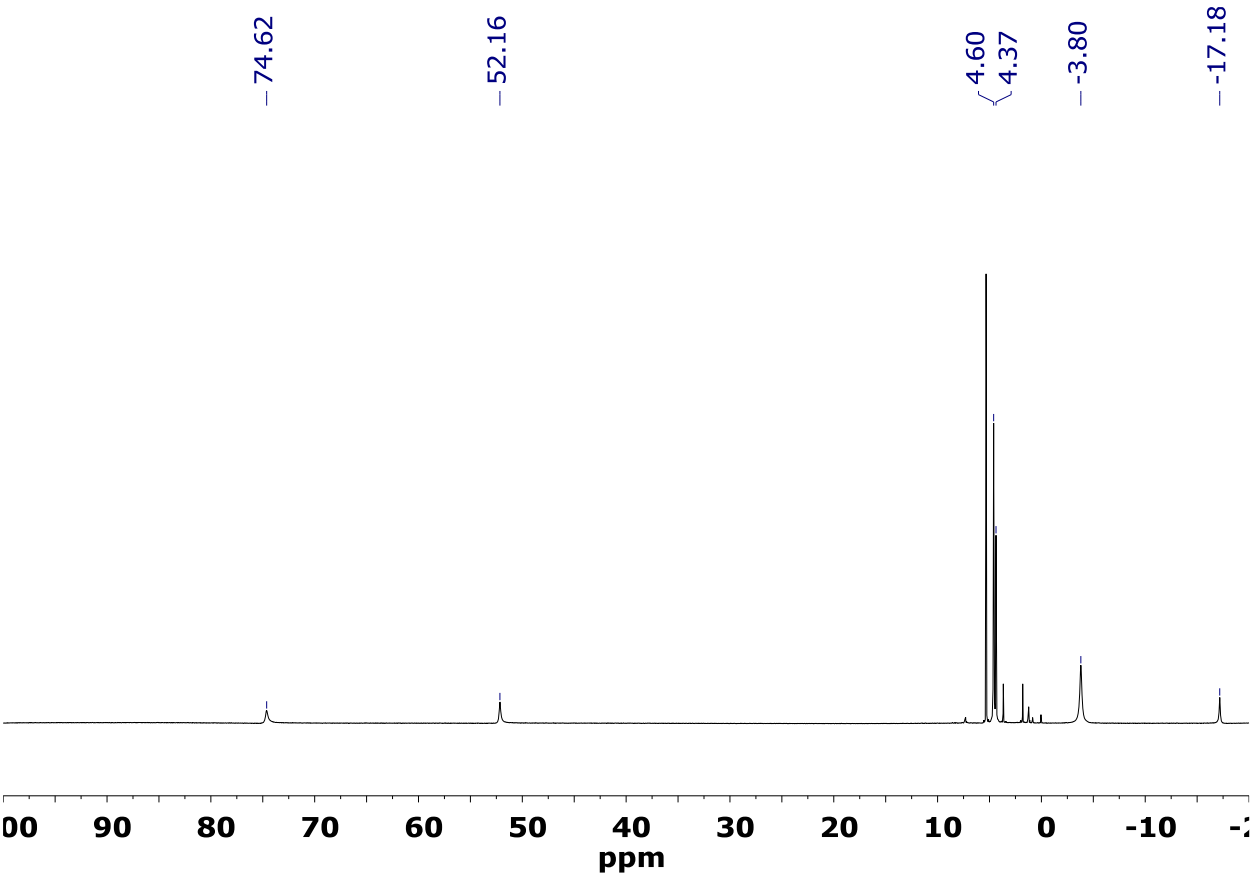

Figure S9. ^{1}H NMR spectrum ($CDCl_3$, 25°C, 399.53 MHz) of Ph_4P_2-bpyFeCl_2 (**1**).

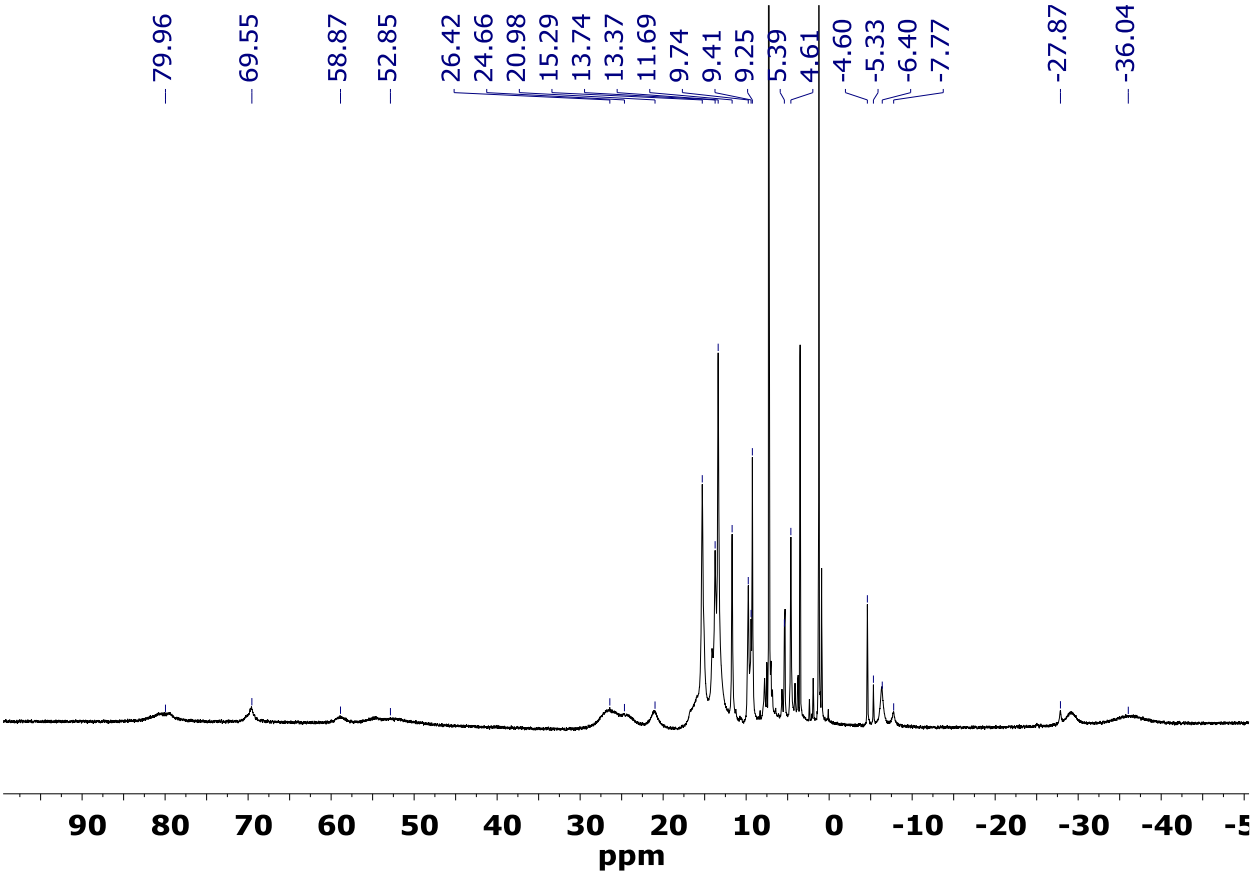

Figure S10. ^{1}H NMR spectrum ($CDCl_3$, 25°C, 399.53 MHz) of **2^{H}**.

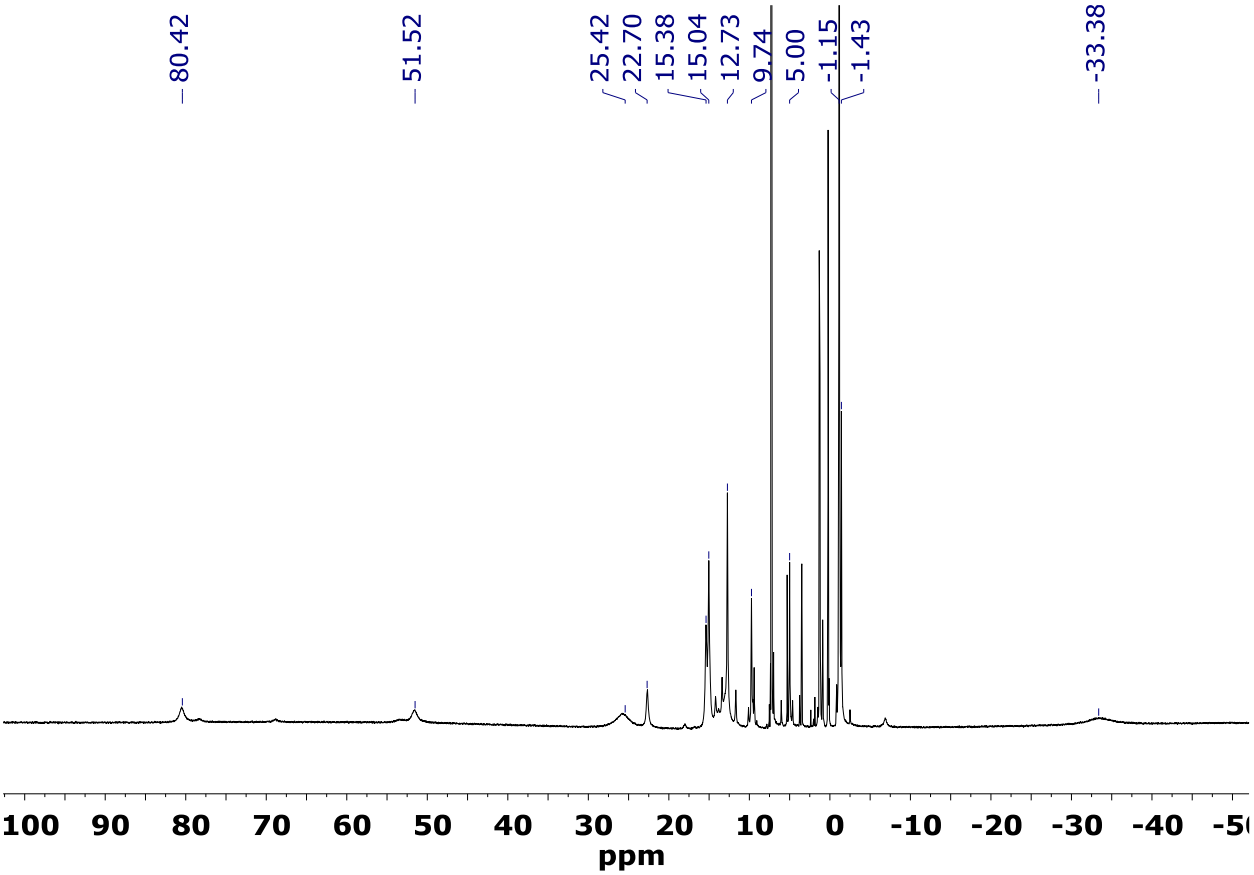

Figure S11. ^{1}H NMR spectrum ($CDCl_3$, 25°C, 399.53 MHz) of **2**^{tBu}.

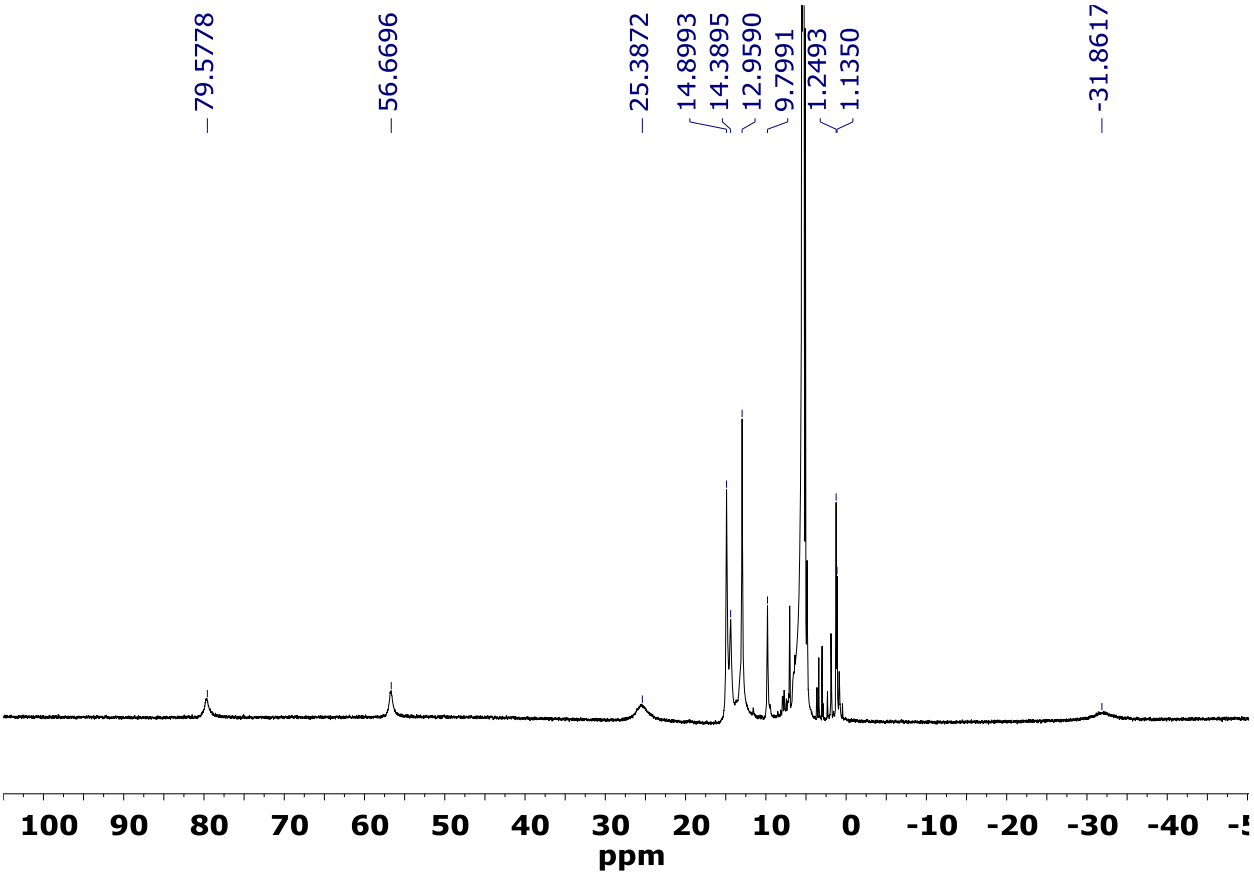

Figure S12. ^{1}H NMR spectrum (CH_2Cl_2, 25°C, 399.53 MHz) of **2**^{CF3}.

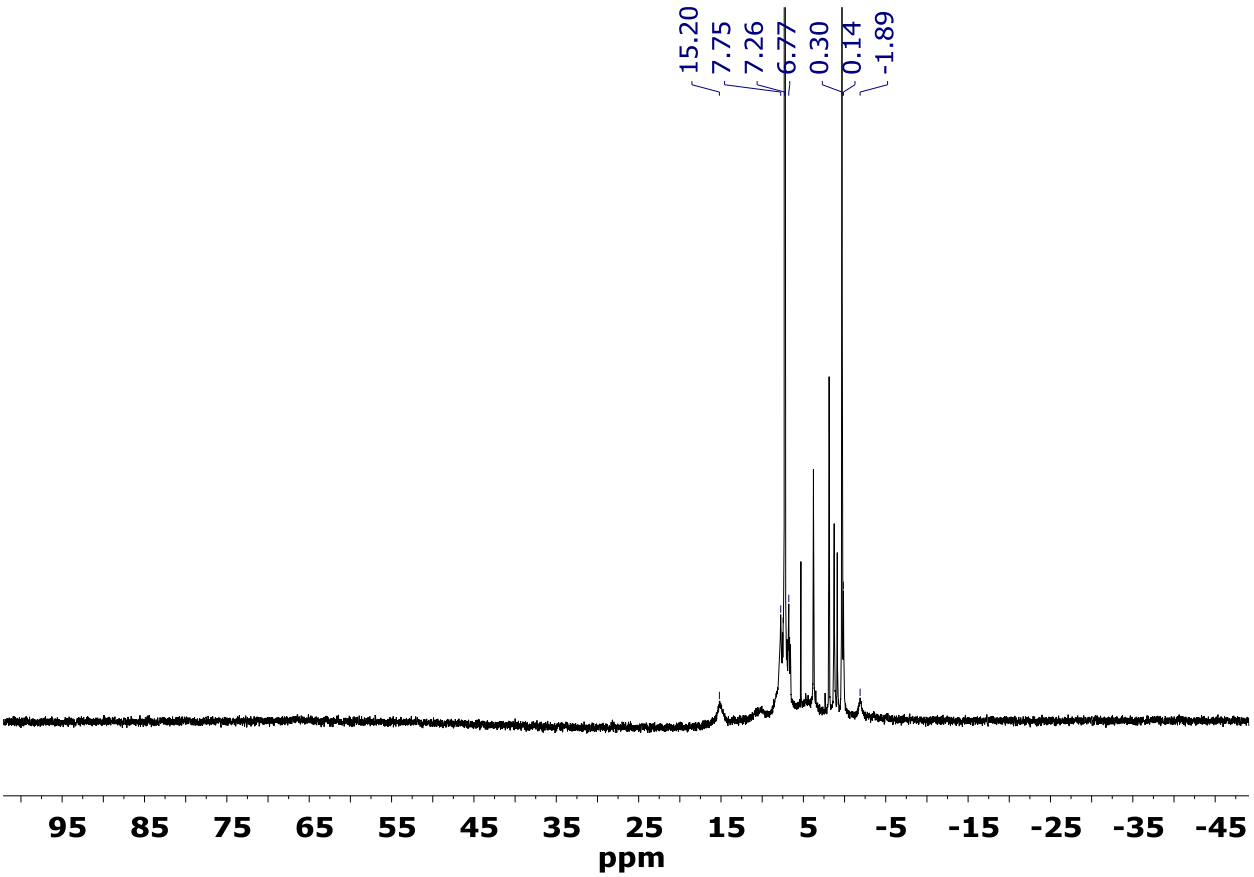

Figure S13. ^{1}H NMR spectrum ($CDCl_3$, 25°C, 399.53 MHz) of $\mathbf{2}^{\mathbf{2\text{-}OH}}$.

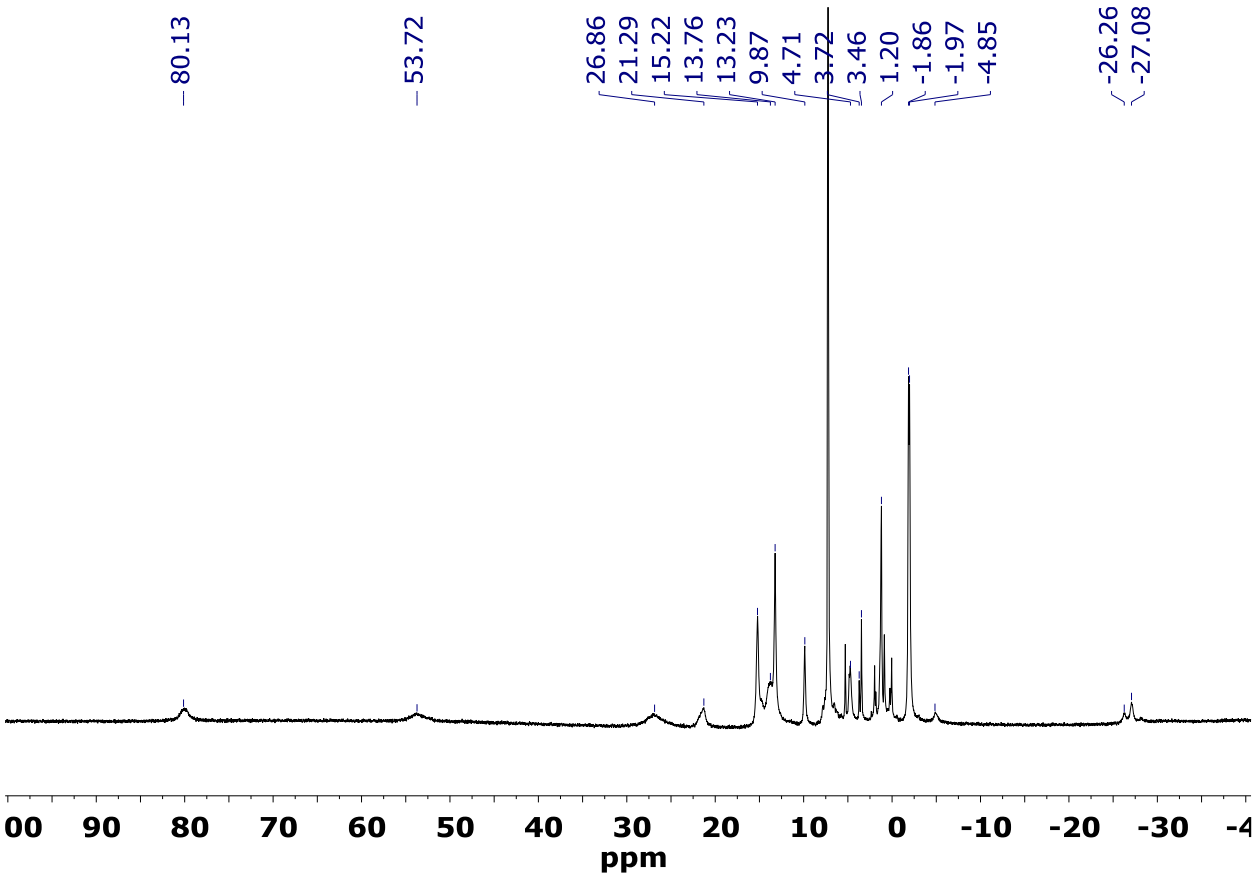

Figure S14. ^{1}H NMR spectrum ($CDCl_3$, 25°C, 399.53 MHz) of $\mathbf{2}^{\mathbf{3\text{-}OH}}$.

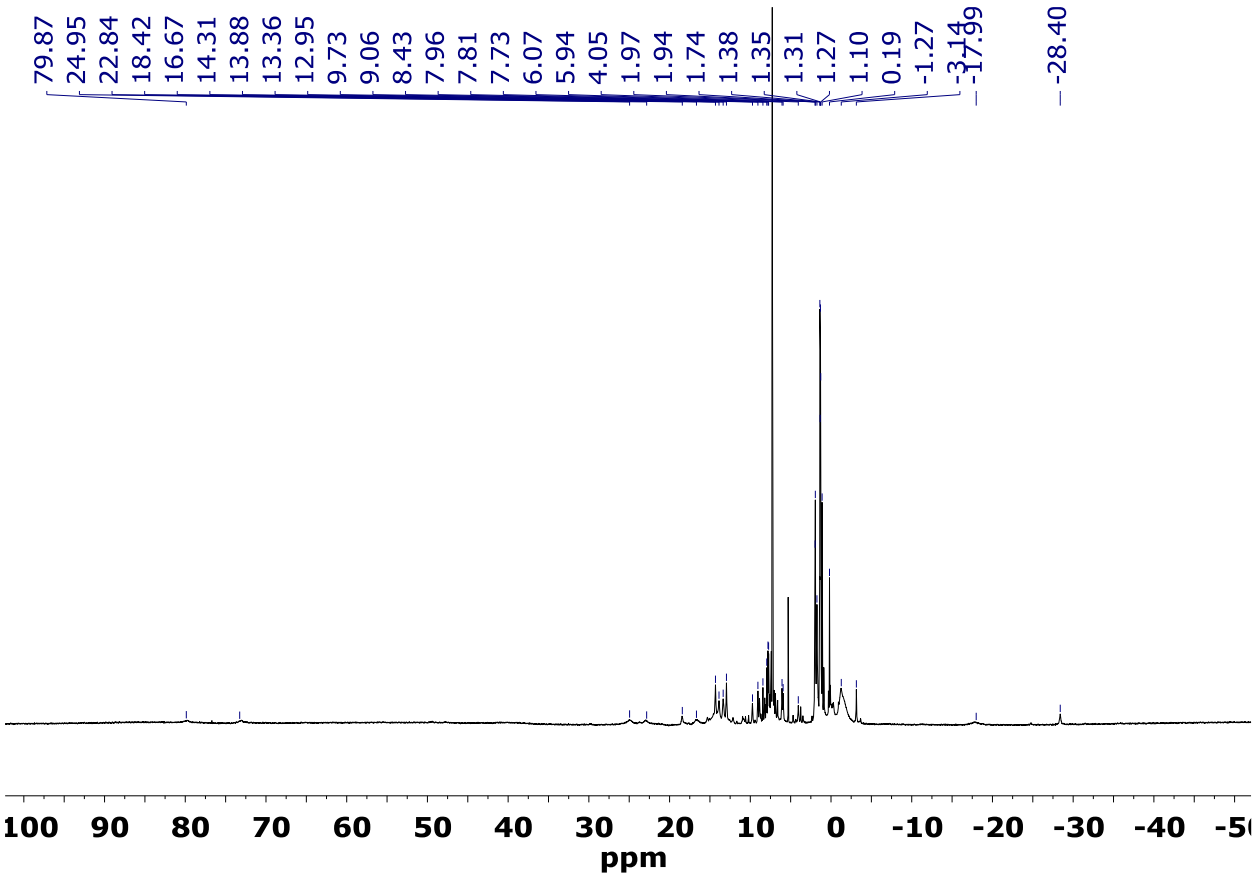

Figure S15. ^{1}H NMR spectrum ($CDCl_3$, 25°C, 399.53 MHz) of $\mathbf{2}^{\mathbf{2\text{-}BPin}}$.

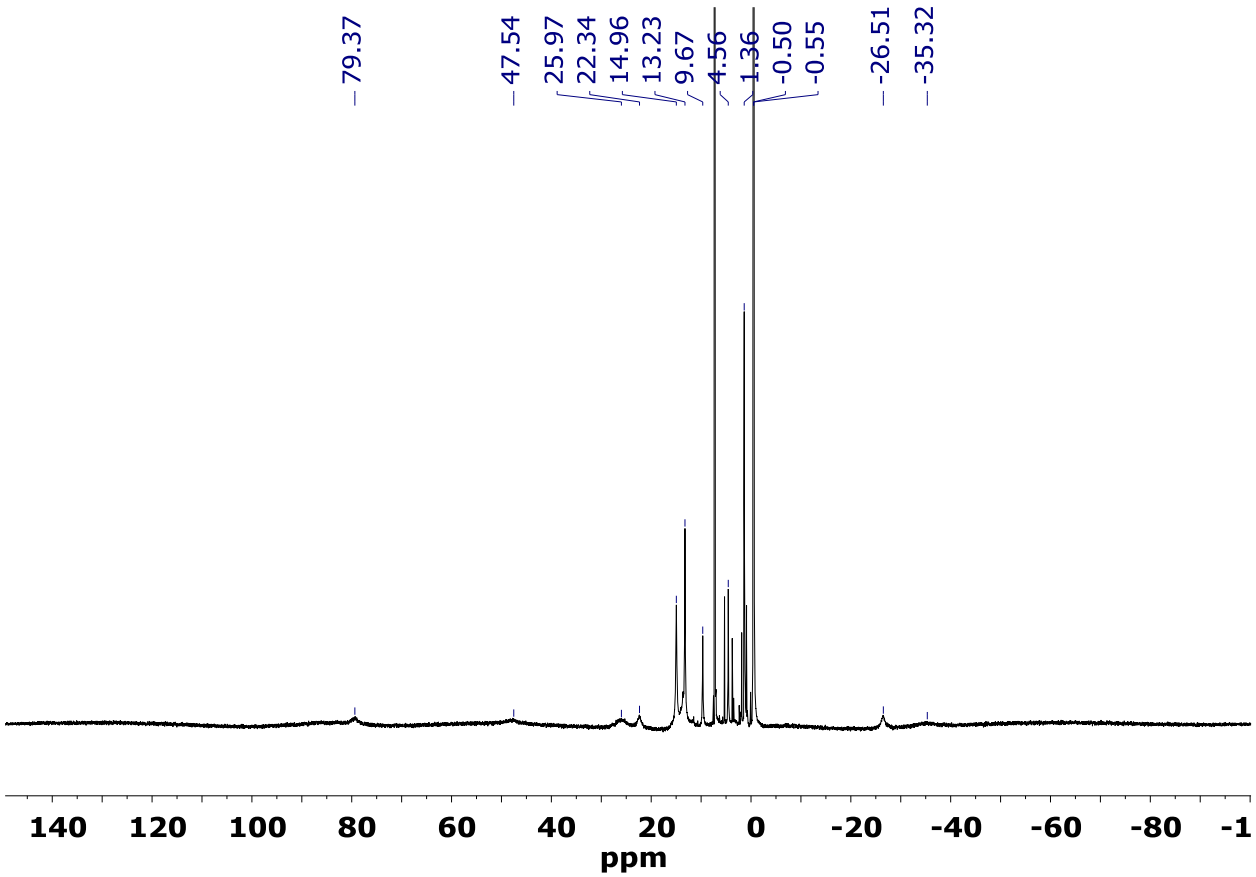

Figure S16. ^{1}H NMR spectrum ($CDCl_3$, 25°C, 399.53 MHz) of **2**$^{\mathbf{3\text{-}BPin}}$.

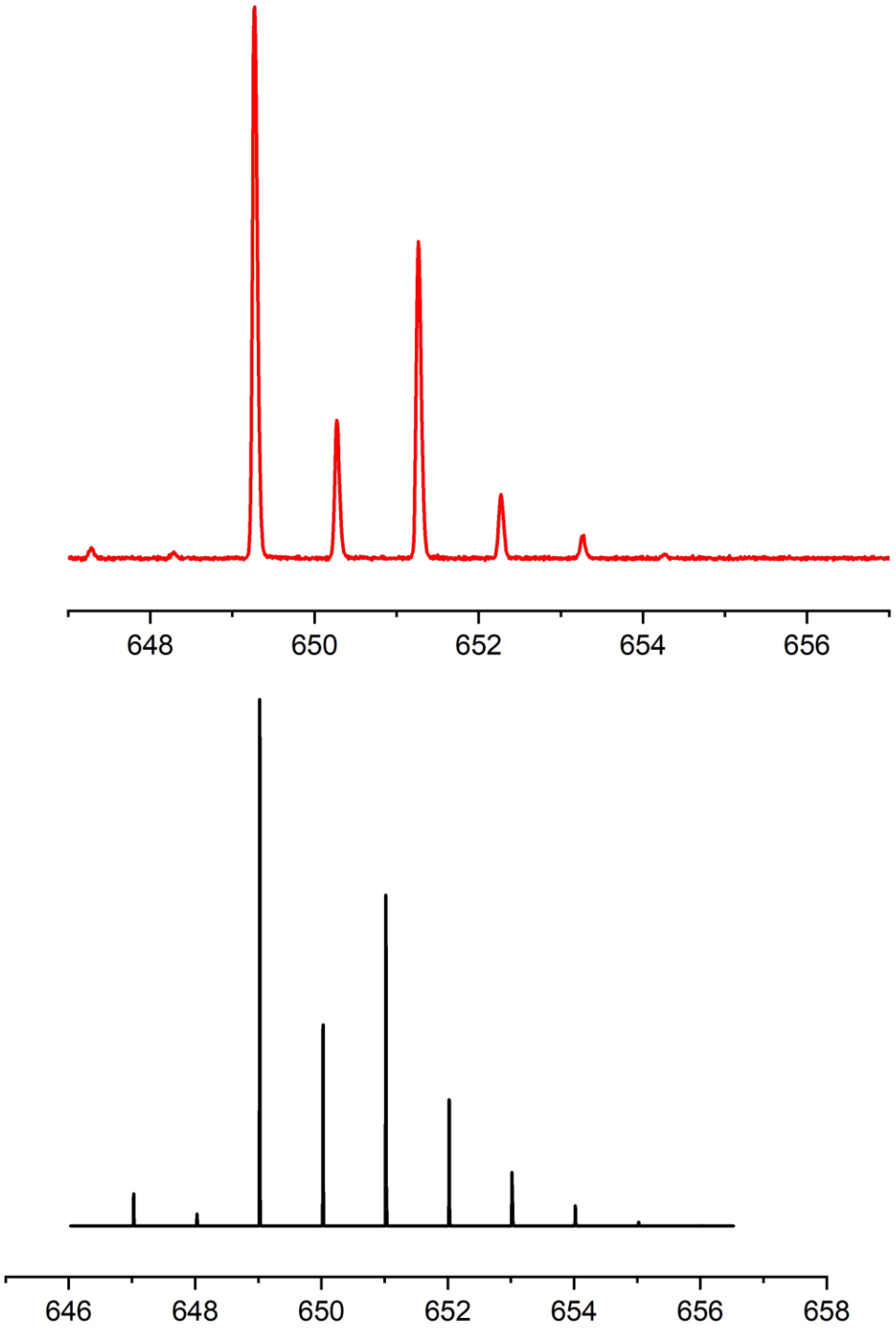

Figure S17. MALDI-TOF spectrum of **Ph_4P_2-bpyFeCl_2** (**1**) (top, red) obtained in an anthracene matrix and the predicted isotopic pattern (bottom, black). Monoisotopic mass for $C_{34}H_{25}Cl_2FeN_2P_2$ (M- H): Calc. Calc.649.018; Found 649.264.

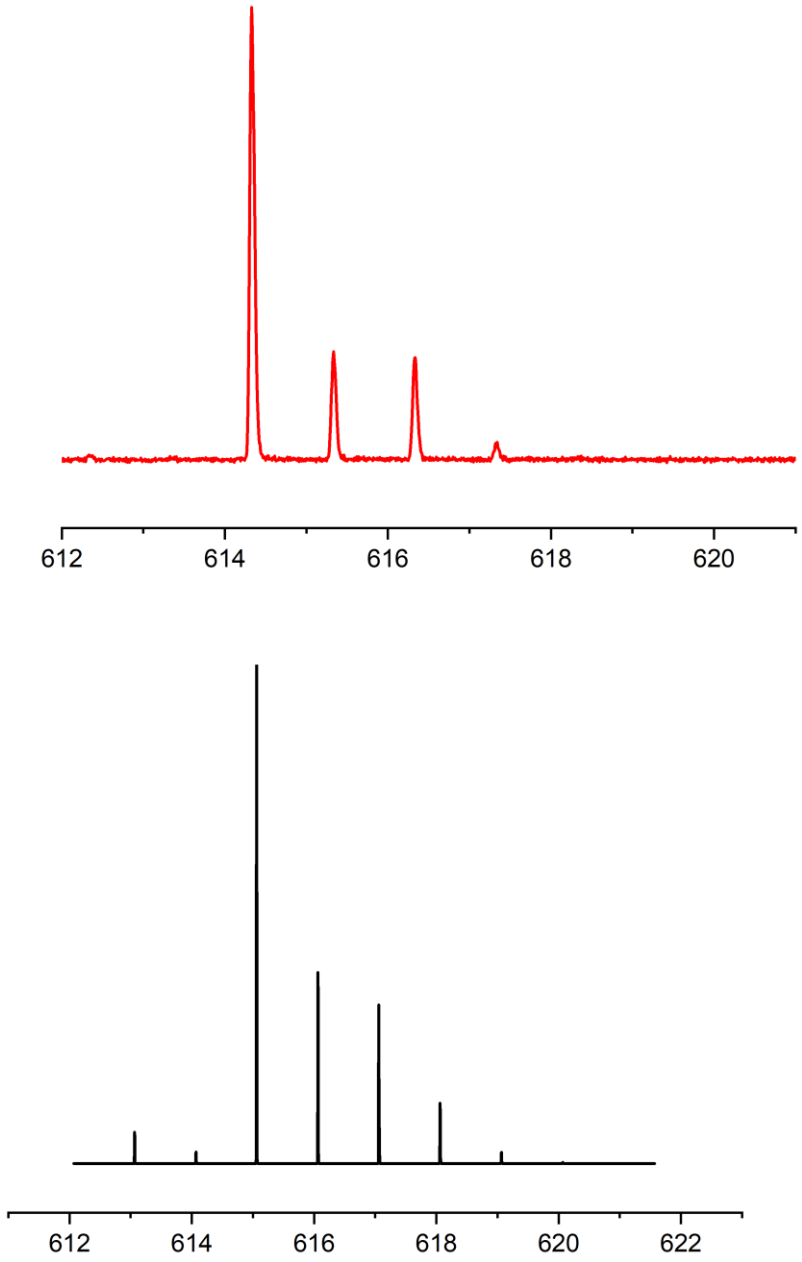

Figure S18. MALDI-TOF spectrum of **Ph_4P_2-bpyFeCl_2** (**1**) (top, red) obtained in an anthracene matrix and the predicted isotopic pattern (bottom, black). Monoisotopic mass for $C_{34}H_{26}ClFeN_2P_2$ (M- Cl): Calc. Calc.615.063; Found 614.329.

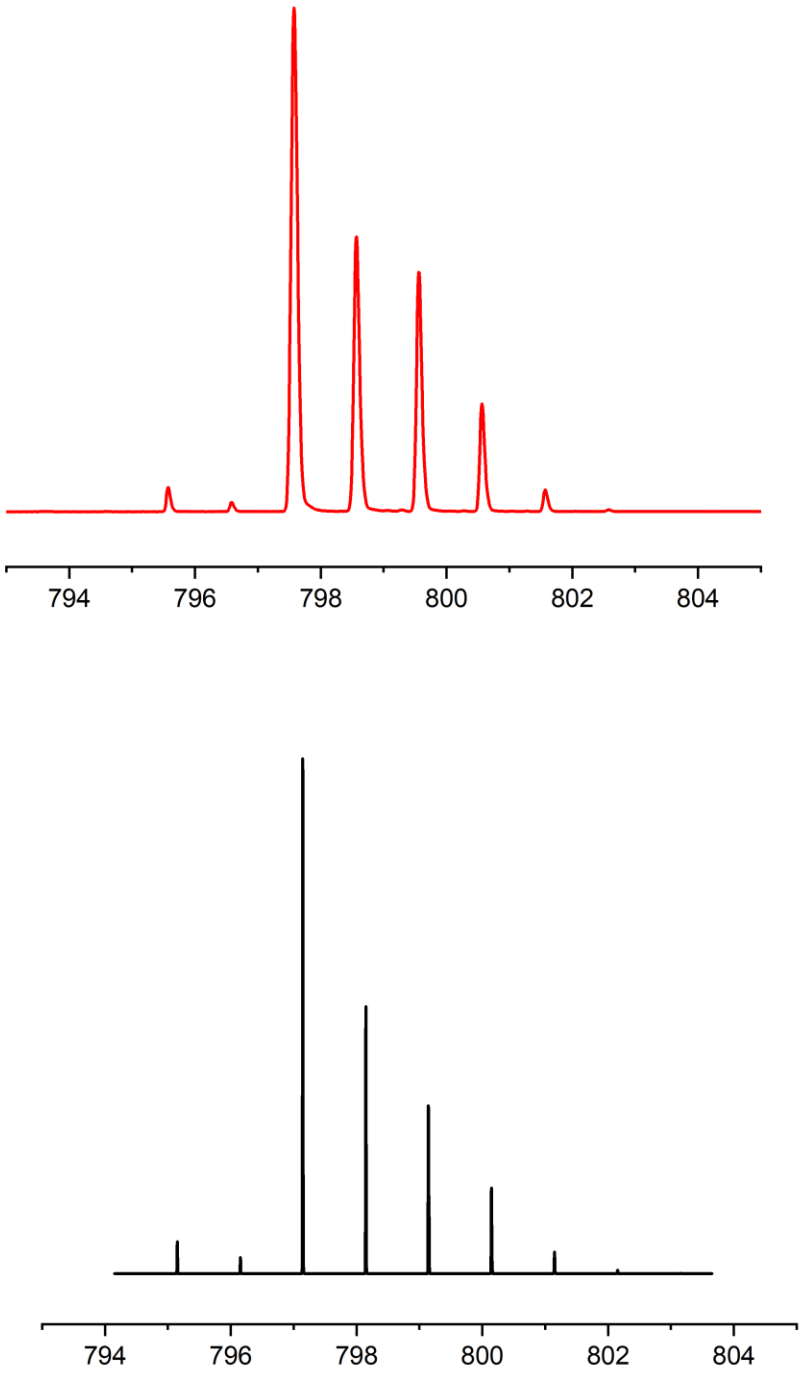

Figure S19. MALDI-TOF spectrum of **2^{H}** (top, red) obtained in an anthracene matrix and the predicted isotopic pattern (bottom, black). Monoisotopic mass for $C_{46}H_{36}ClFeN_4P_2$ (M- PF_6): Calc. 797.148; Found 797.576.

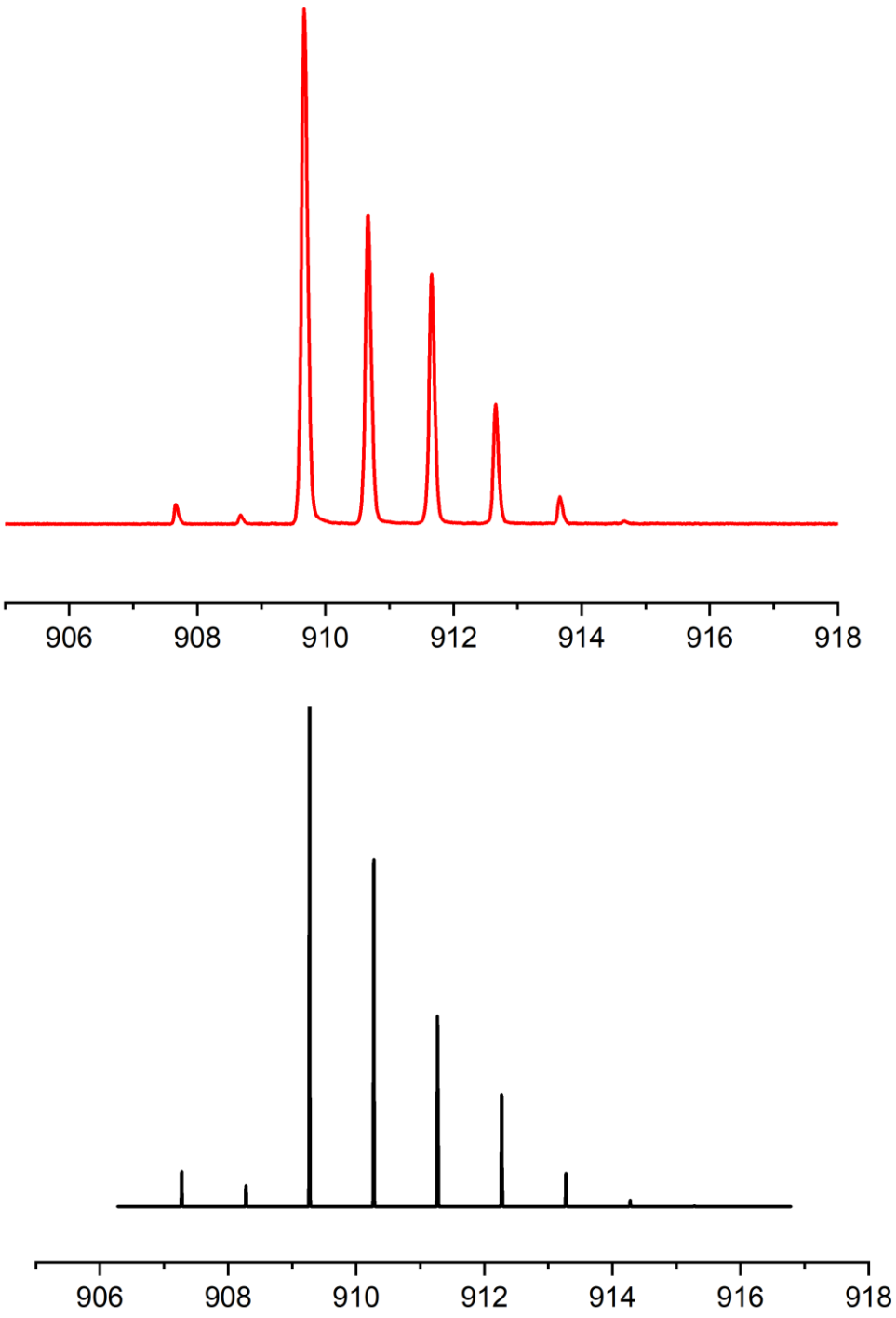

Figure S20. MALDI-TOF spectrum of **2**^{tBu} (top, red) obtained in an anthracene matrix and the predicted isotopic pattern (bottom, black). Monoisotopic mass for $C_{54}H_{52}ClFeN_4P_2$ (M- PF_6): Calc. 909.659; Found 909.271.

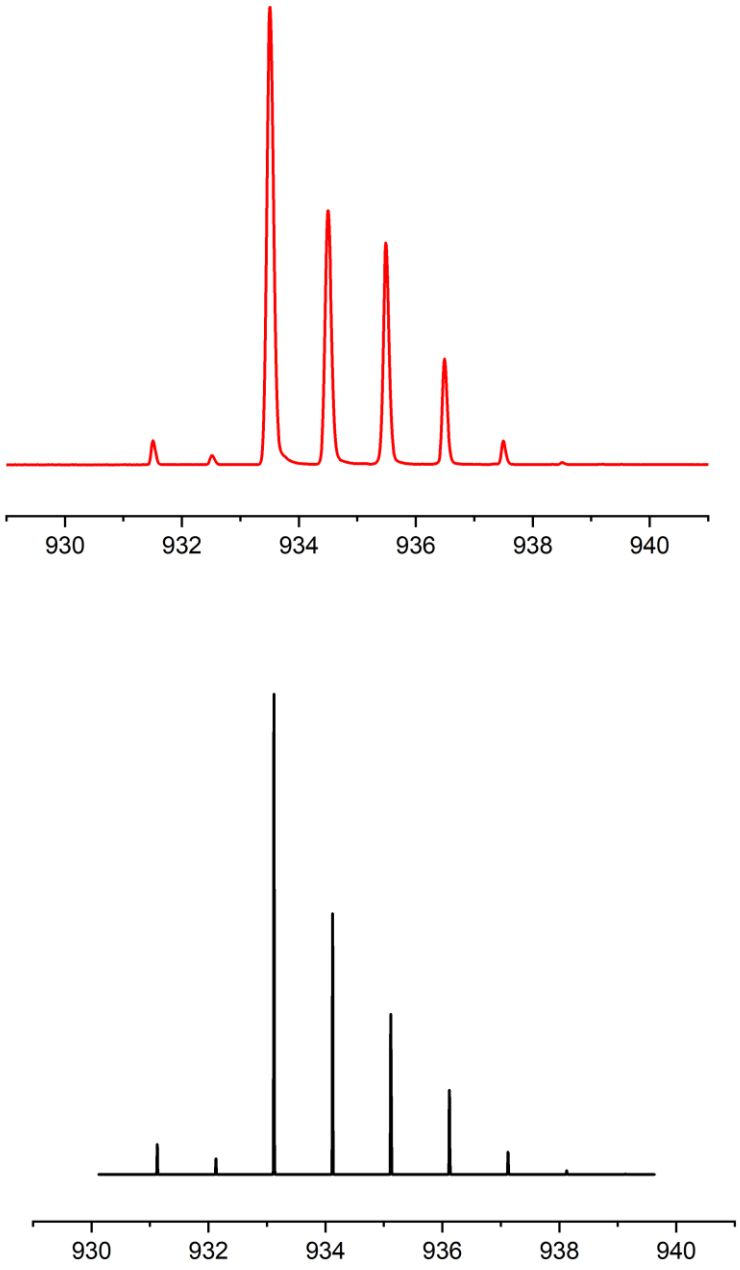

Figure S21. MALDI-TOF spectrum of **2**^{CF3} (top, red) obtained in an anthracene matrix and the predicted isotopic pattern (bottom, black). Monoisotopic mass for $C_{48}H_{34}ClF_6FeN_4P_2$ (M- PF_6): Calc. 933.120; Found 933.502.

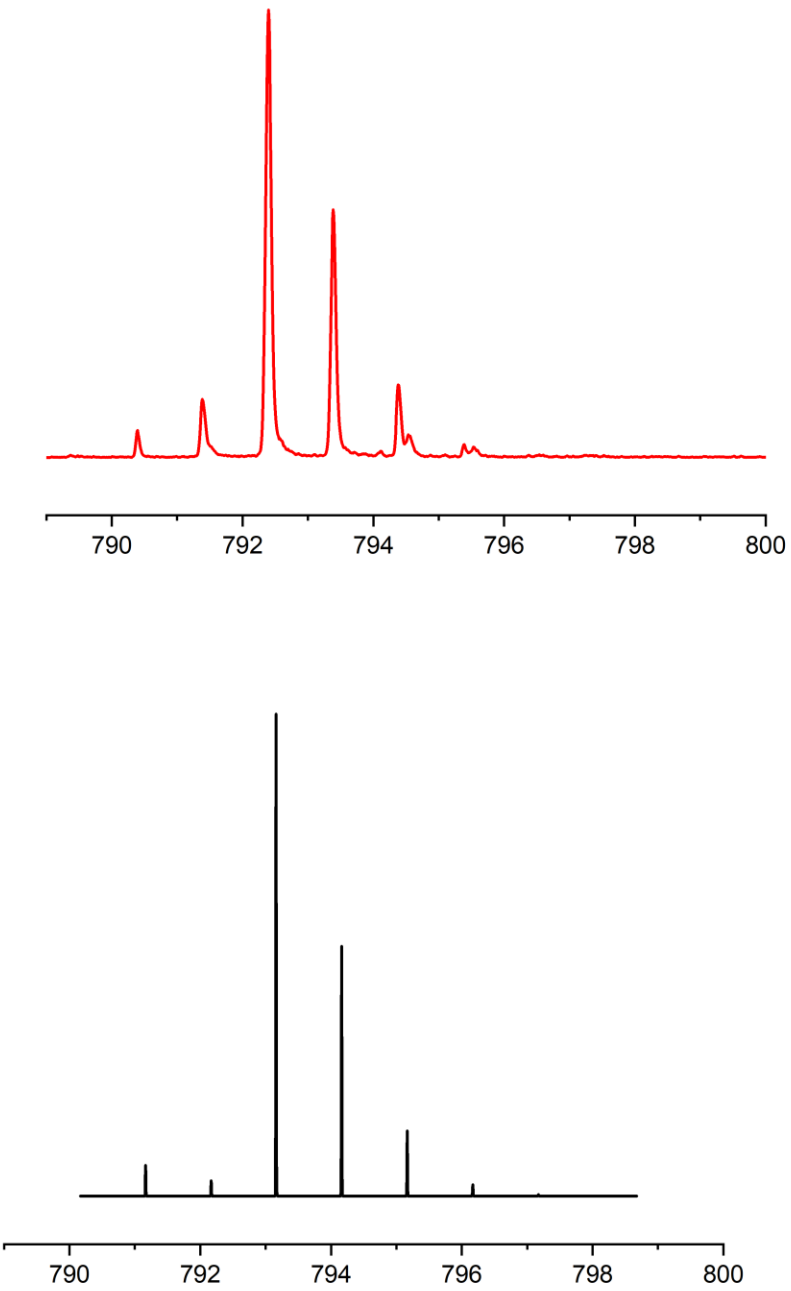

Figure S22. MALDI-TOF spectrum of $\mathbf{2^{2\text{-}OH}}$ (top, red) obtained in an anthracene matrix and the predicted isotopic pattern (bottom, black). Monoisotopic mass for $C_{46}H_{35}FeN_4O_2P_2$ (M- (HCL +PF_6)): Calc. 793.158; Found 792.405.

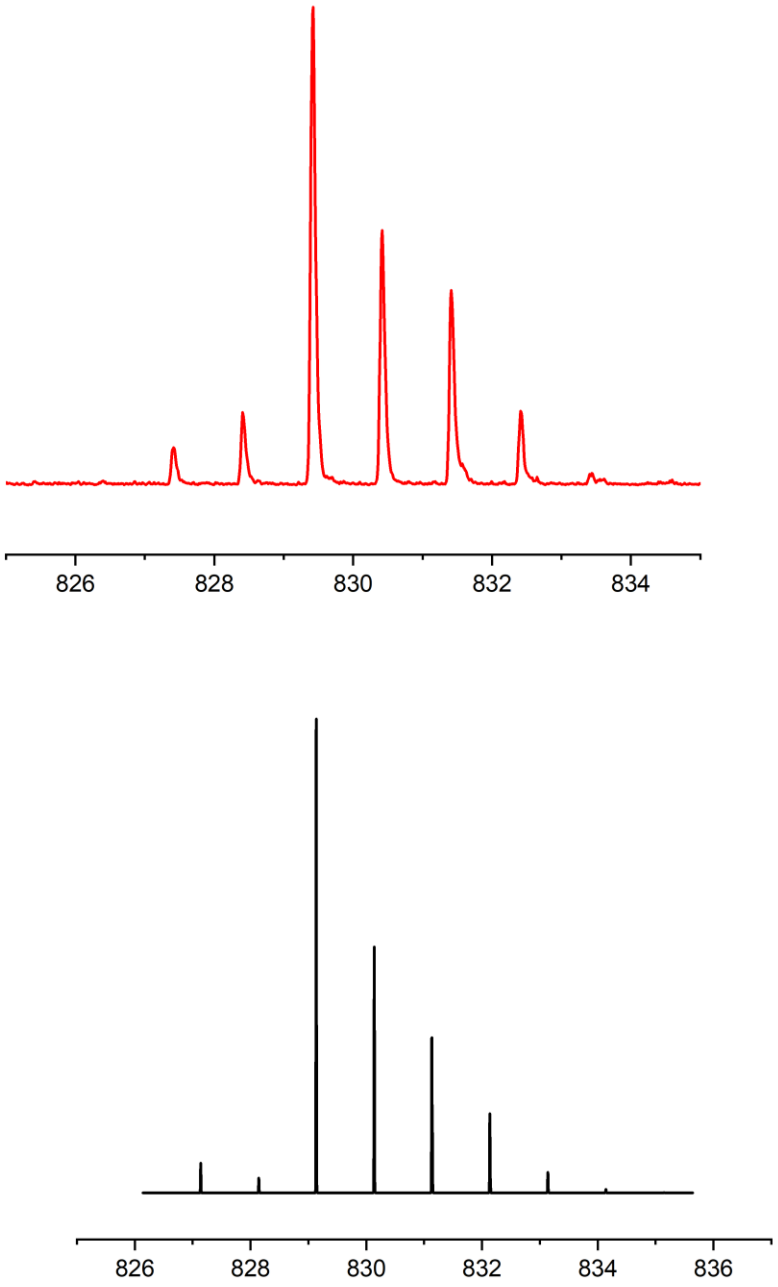

Figure S23. MALDI-TOF spectrum of $\mathbf{2}^{\mathbf{3\text{-}OH}}$ (top, red) obtained in an anthracene matrix and the predicted isotopic pattern (bottom, black). Monoisotopic mass for $C_{46}H_{35}FeN_4O_2P_2$ (M- PF_6): Calc. 829.135; Found 829.414.

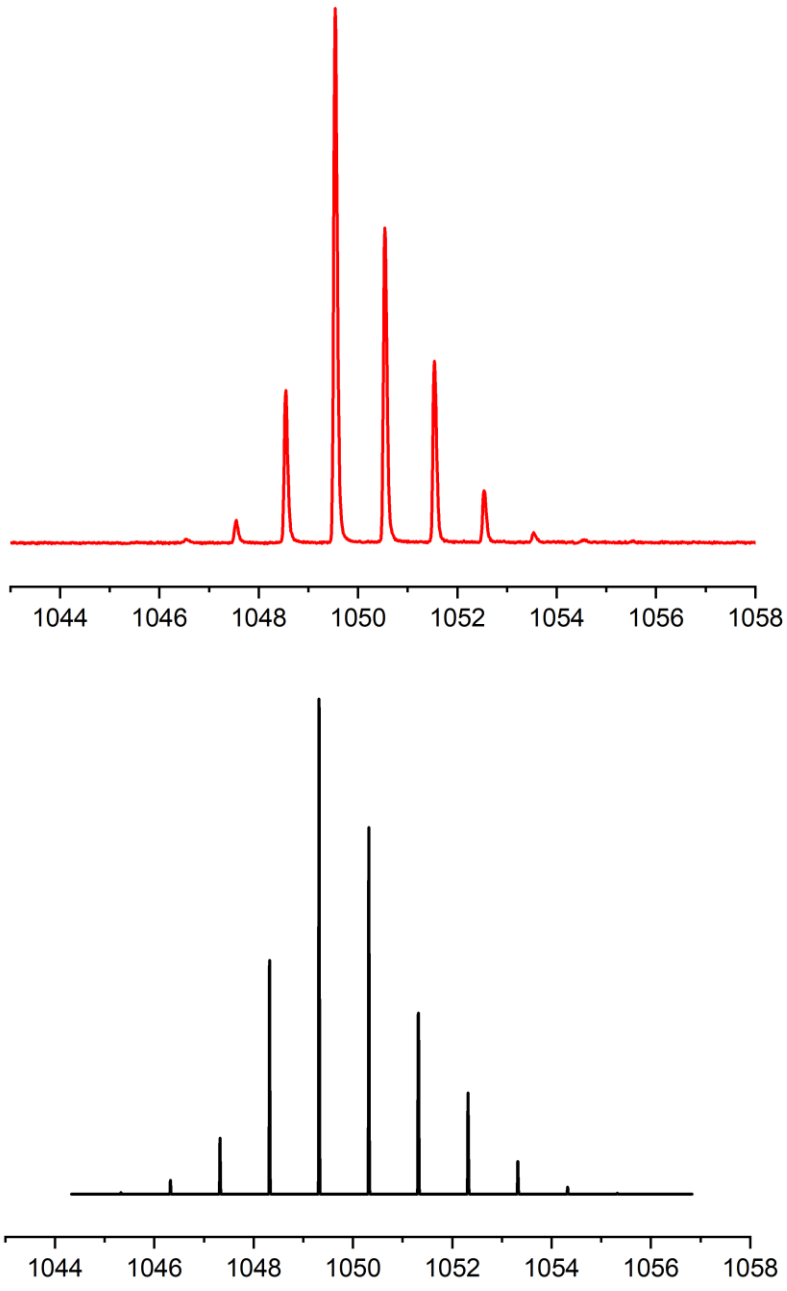

Figure S24. MALDI-TOF spectrum of $\mathbf{2}^{\mathbf{2\text{-}BPin}}$ (top, red) obtained in an anthracene matrix and the predicted isotopic pattern (bottom, black). Monoisotopic mass for $C_{58}H_{58}B_2ClFeN_4O_4P_2$ (M- PF_6): Calc. 1049.316; Found 1049.542.

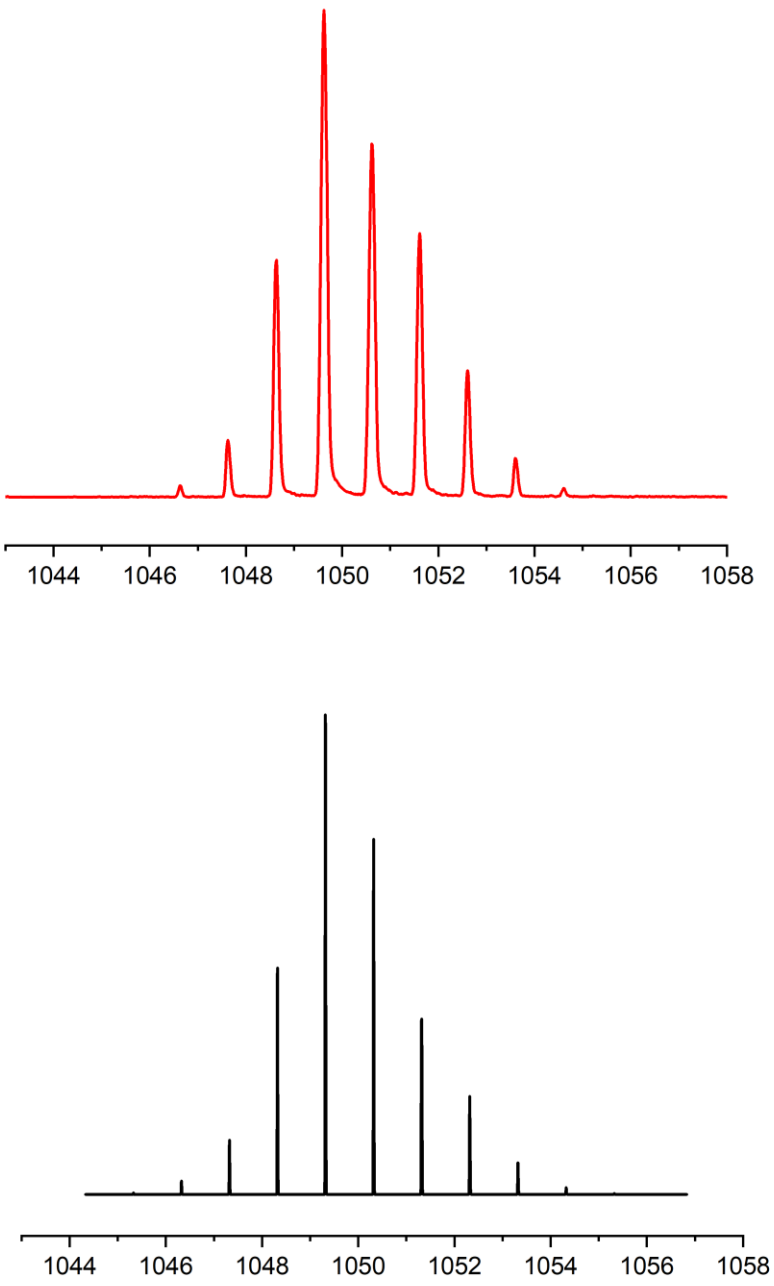

Figure S25. MALDI-TOF spectrum of $\mathbf{2}^{\mathbf{3\text{-}BPin}}$ (top, red) obtained in an anthracene matrix and the predicted isotopic pattern (bottom, black). Monoisotopic mass for $C_{58}H_{58}B_2ClFeN_4O_4P_2$ (M- PF_6): Calc. 1049.316; Found 1049.632.

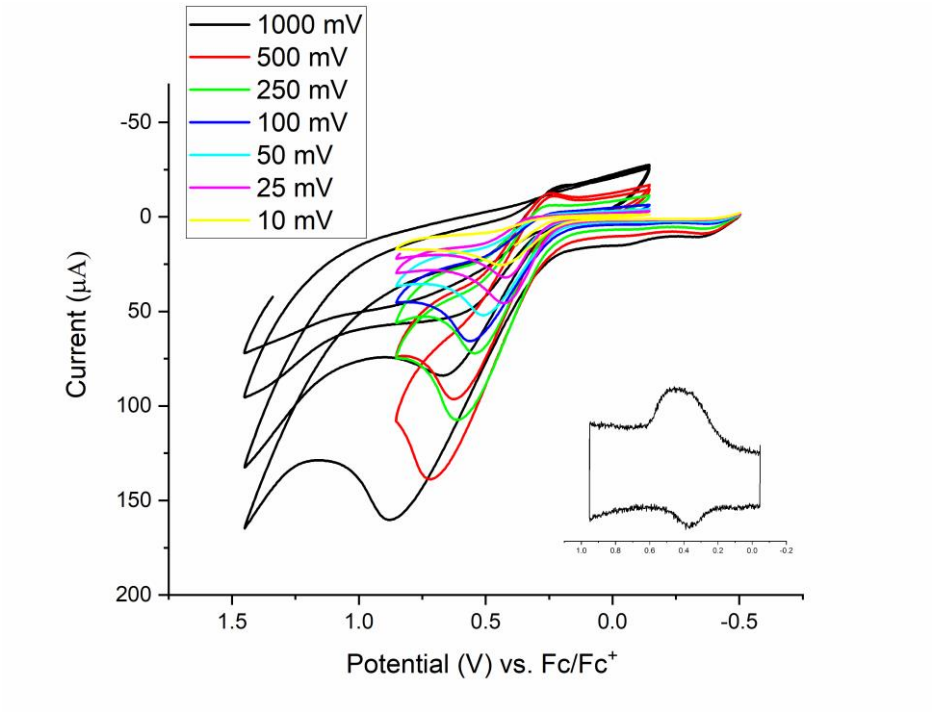

Figure S26. Scan rate dependence of the reductive wave of **Ph_4P_2-bpyFeCl_2** (**1**) (4.40 mM) recorded in CH_2Cl_2 with 0.10 M $[Bu_4N][PF_6]$ at ambient temperature.

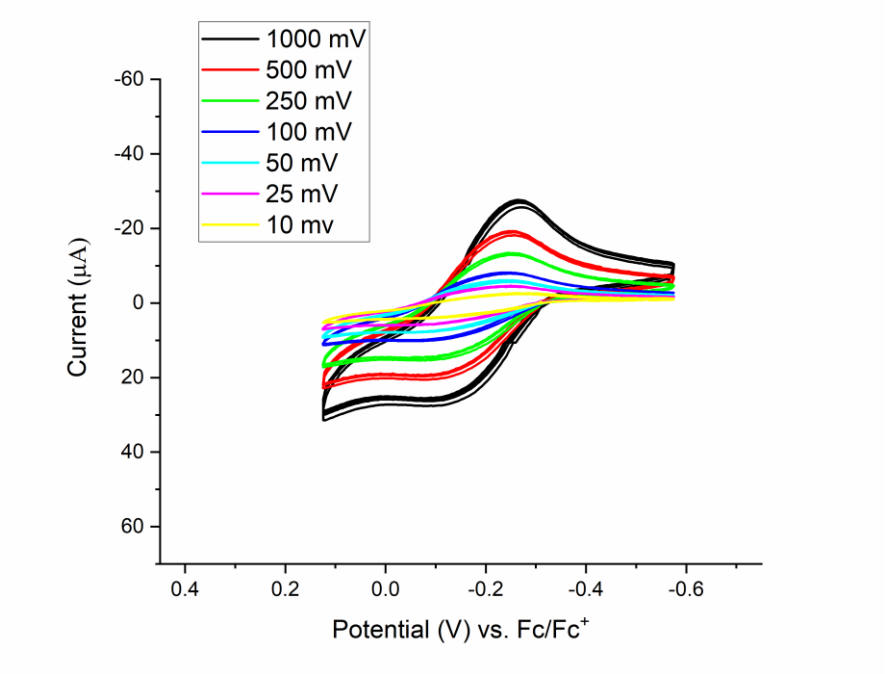

Figure S27. Scan rate dependence of the reductive wave of **Ph_4P_2-bpyFeCl_2** (**1**) (2.30 mM) dissolved in minimum CH_2Cl_2 and recorded in CH_3CN with 0.10 M $[Bu_4N][PF_6]$ at ambient temperature.

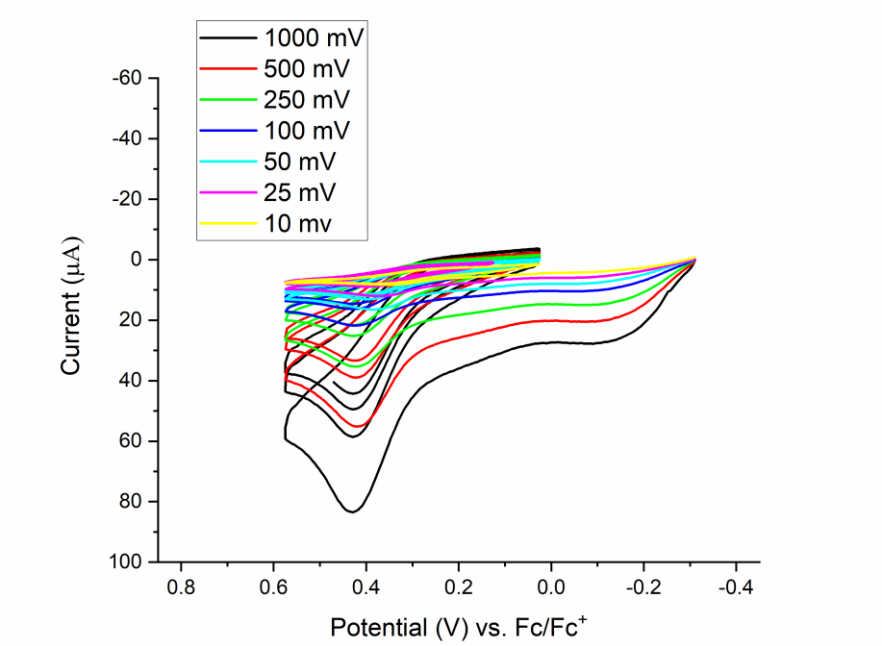

Figure S28. Scan rate dependence of the reductive wave of **Ph_4P_2-bpyFeCl_2** (**1**) (2.30 mM) dissolved in minimum CH_2Cl_2 recorded in CH_3CN with 0.10 M $[Bu_4N][PF_6]$ at ambient temperature.

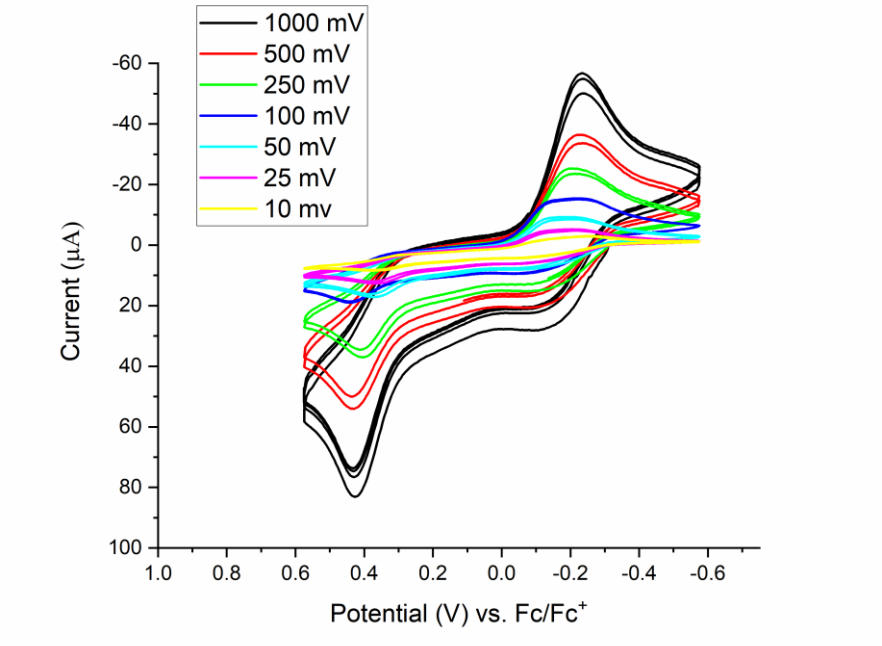

Figure S29. Scan rate dependence of the reductive wave of **Ph_4P_2-bpyFeCl_2** (**1**) (2.30 mM) dissolved in minimum CH_2Cl_2 recorded in CH_3CN with 0.10 M $[Bu_4N][PF_6]$ at ambient temperature.

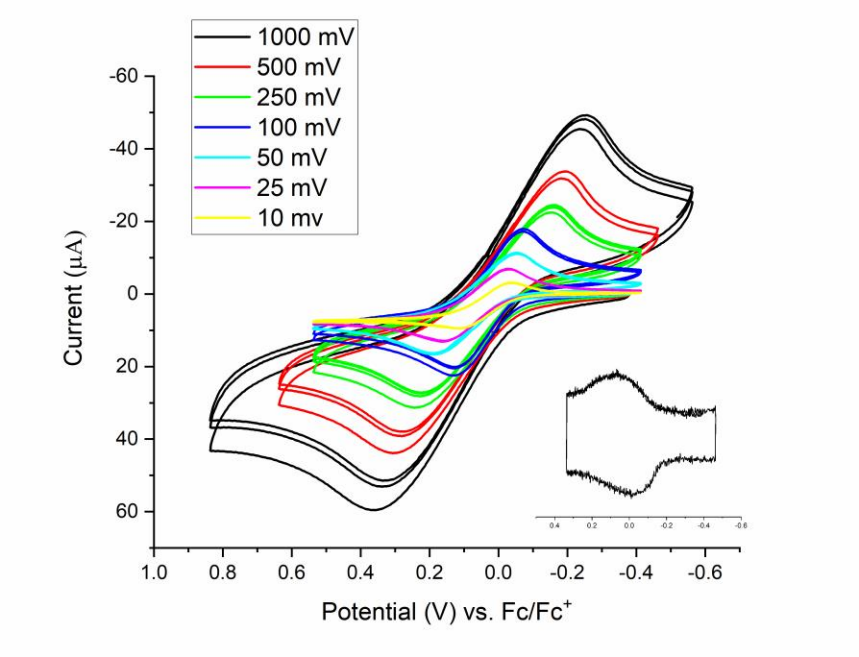

Figure S30. Scan rate dependence of the reductive wave of **2^{H}** (1.13 mM) recorded in CH_2Cl_2 with 0.10 M $[Bu_4N][PF_6]$ at ambient temperature. Nonlinear response due to the evaporation of CH_2Cl_2 solvent.

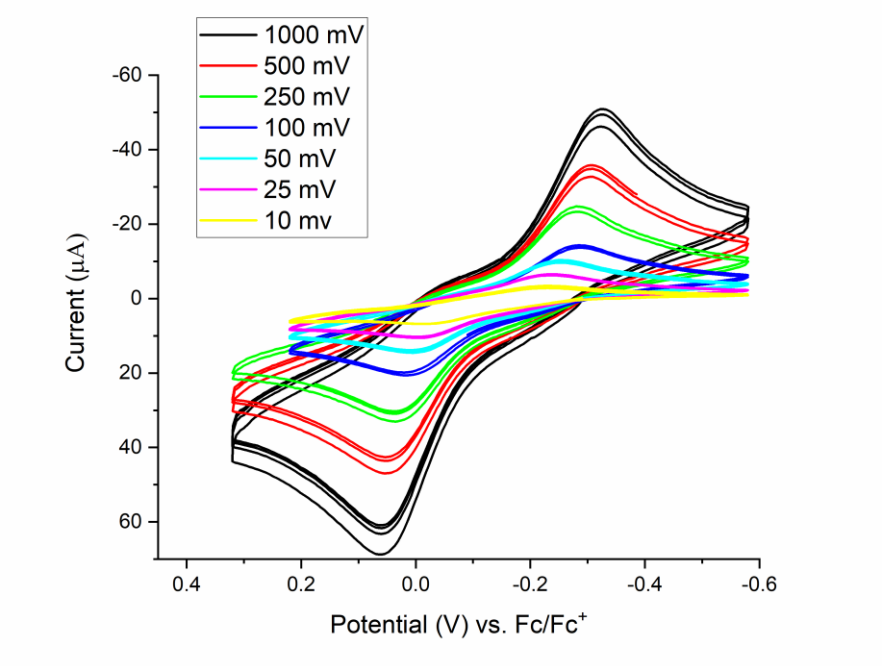

Figure S31. Scan rate dependence of the reductive wave of **2^{H}** (2.83 mM) recorded in CH_3CN with 0.10 M $[Bu_4N][PF_6]$ at ambient temperature.

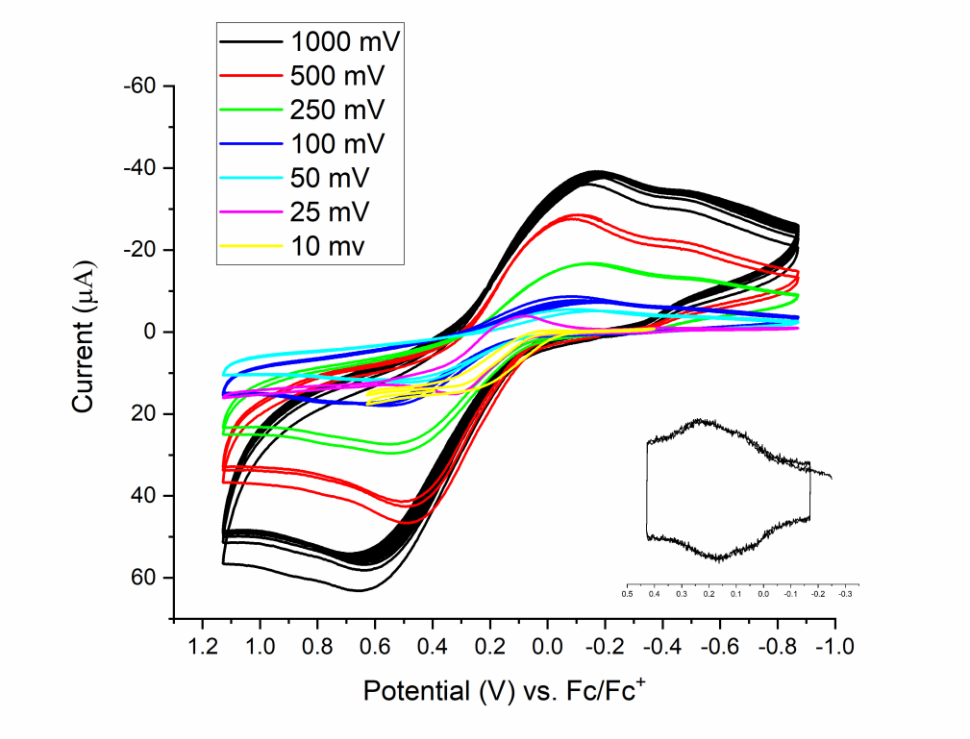

Figure S32. Scan rate dependence of the reductive wave of **2**^{tBu} (1.40 mM) recorded in CH_2Cl_2 with 0.10 M $[Bu_4N][PF_6]$ at ambient temperature. Nonlinear response due to the evaporation of CH_2Cl_2 solvent.

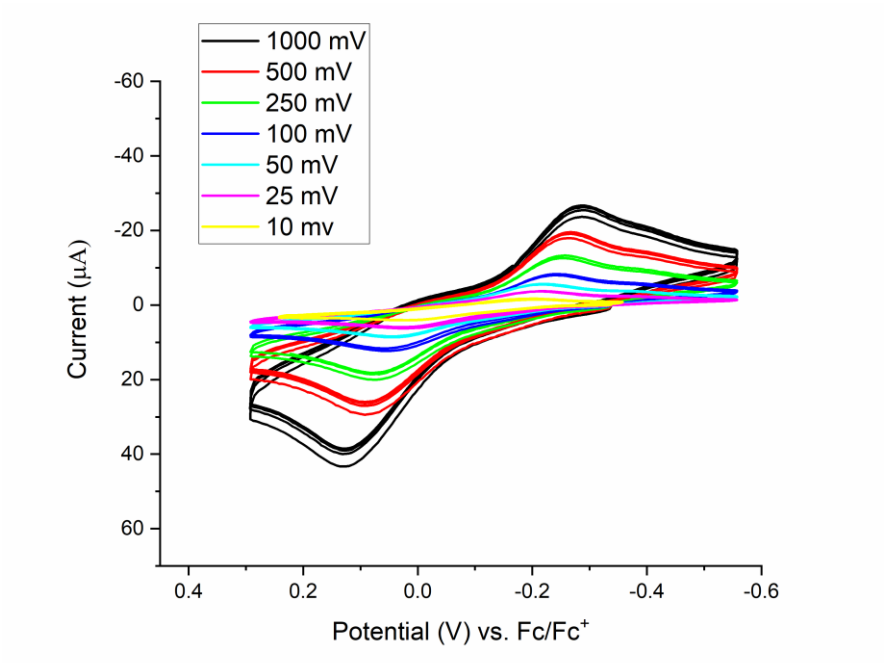

Figure S33. Scan rate dependence of the reductive wave of **2**^{tBu} (1.90 mM) recorded in CH_3CN with 0.10 M $[Bu_4N][PF_6]$ at ambient temperature.

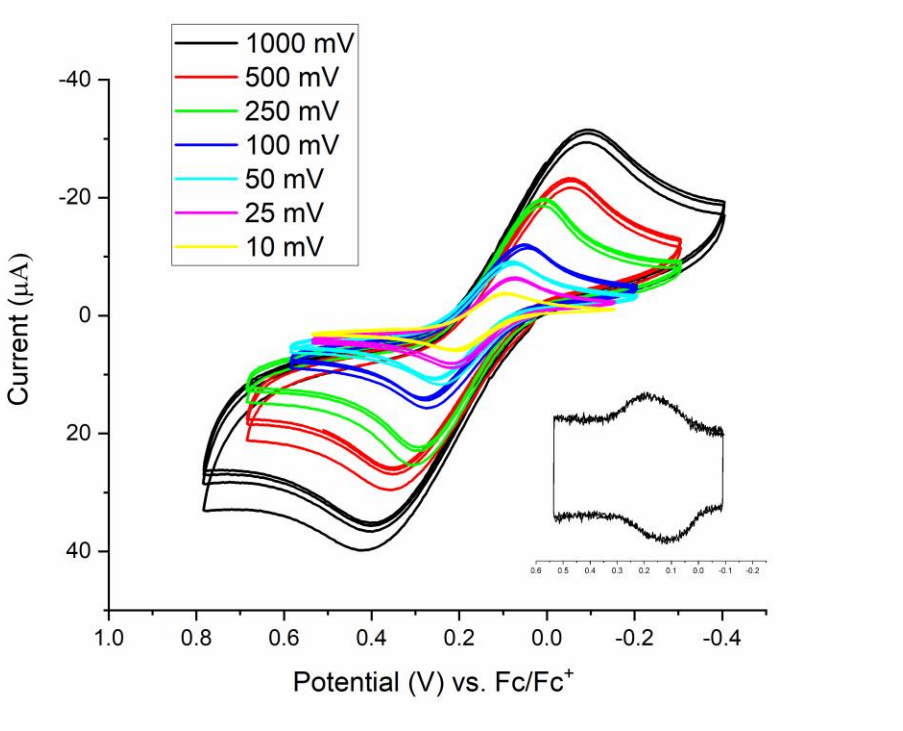

Figure S34. Scan rate dependence of the reductive wave of **2**^{CF3} (1.48 mM) recorded in CH_2Cl_2 with 0.10 M $[Bu_4N][PF_6]$ at ambient temperature.

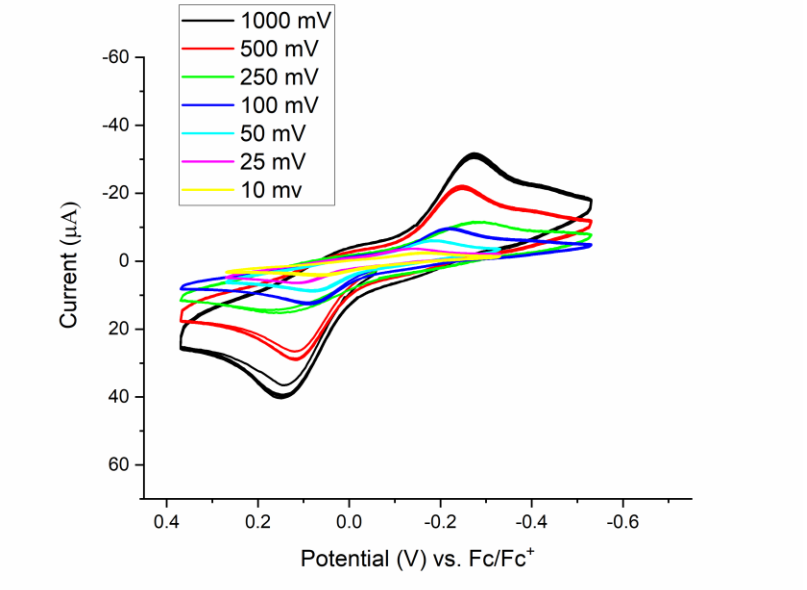

Figure S35. Scan rate dependence of the reductive wave of **2**^{CF3} (2.47 mM) recorded in CH_3CN with 0.10 M $[Bu_4N][PF_6]$ at ambient temperature.

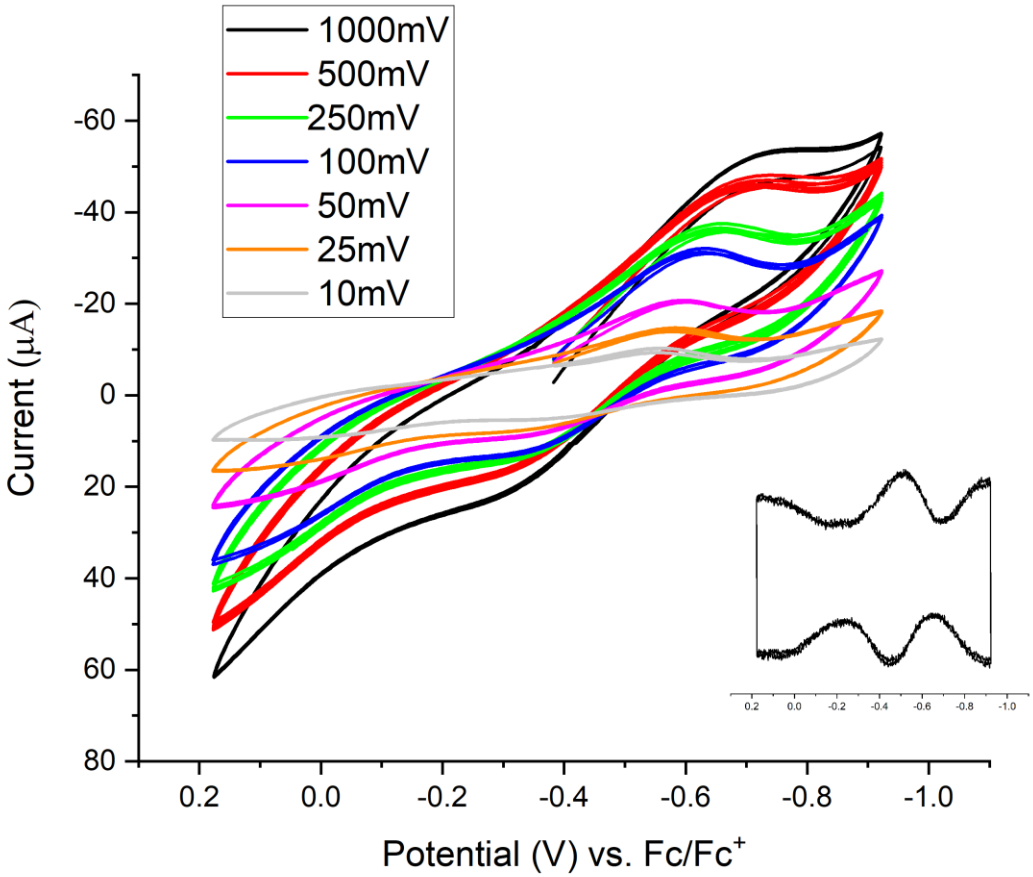

Figure S36. Scan rate dependence of the reductive wave of $\mathbf{2}^{\mathbf{2\text{-}OH}}$ (6.26 mM) recorded in CH_2Cl_2 with 0.10 M $[Bu_4N][PF_6]$ at ambient temperature. Square wave parameters: amplitude = 20 mV; period = 0.02 seconds; increment = 2 mV; sampling width = 0.001.

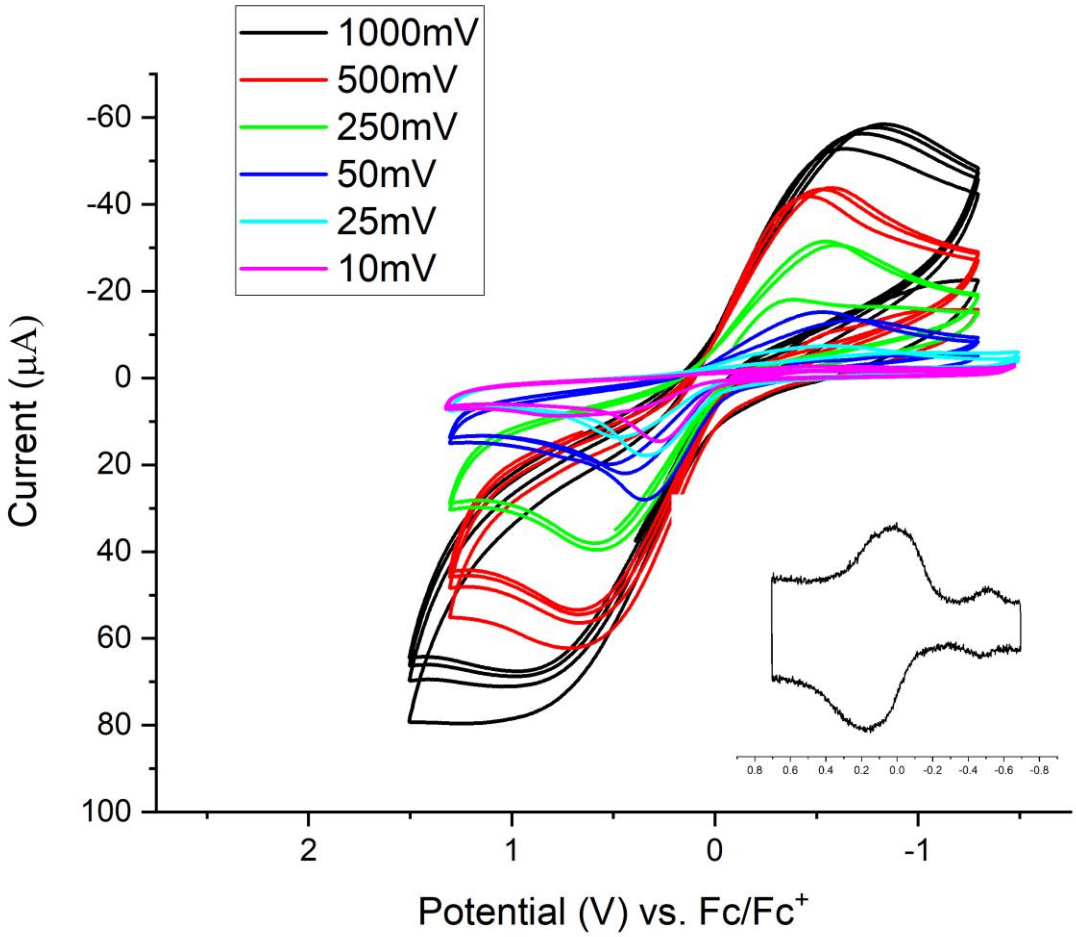

Figure S37. Scan rate dependence of the reductive wave of $\mathbf{2}^{\mathbf{3\text{-}OH}}$ (7.39 mM) recorded in CH_2Cl_2 with 0.10 M $[Bu_4N][PF_6]$ at ambient temperature. Square wave parameters: amplitude = 20 mV; period = 0.02 seconds; increment = 2 mV; sampling width = 0.001.

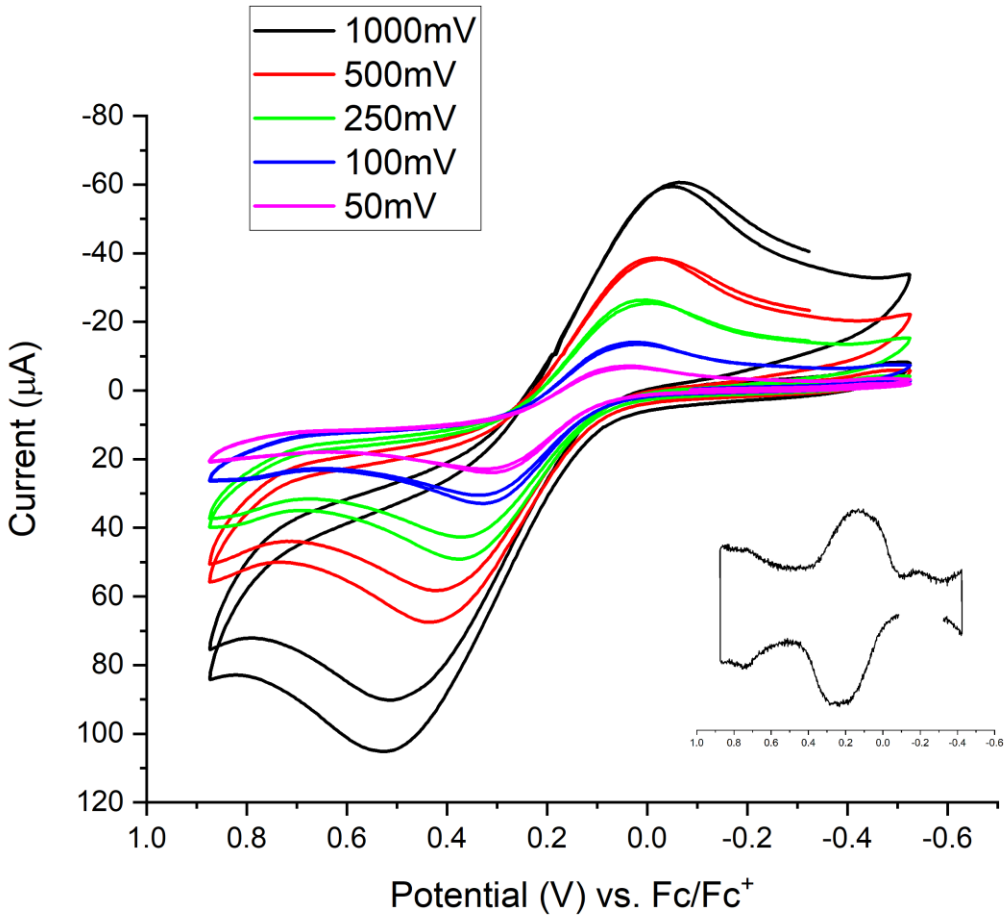

Figure S38. Scan rate dependence of the reductive wave of $\mathbf{2}^{\mathbf{2\text{-}BPin}}$ (5.44 mM) recorded in CH_2Cl_2 with 0.10 M $[Bu_4N][PF_6]$ at ambient temperature. Square wave parameters: amplitude = 20 mV; period = 0.02 seconds; increment = 2 mV; sampling width = 0.001.

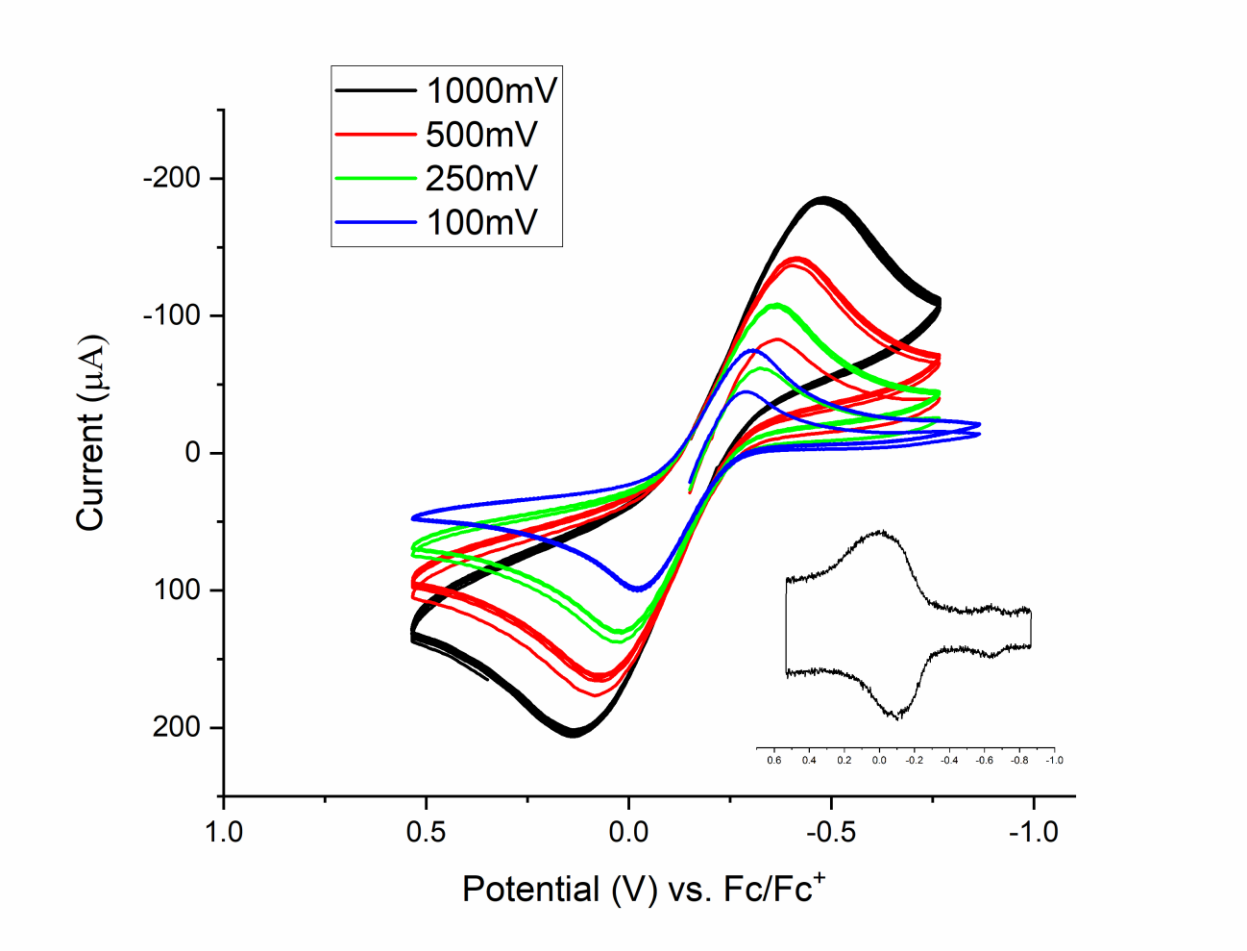

Figure S39. Scan rate dependence of the reductive wave of $\mathbf{2}^{\mathbf{3\text{-}BPin}}$ (6.86 mM) recorded in CH_2Cl_2 with 0.10 M $[Bu_4N][PF_6]$ at ambient temperature.

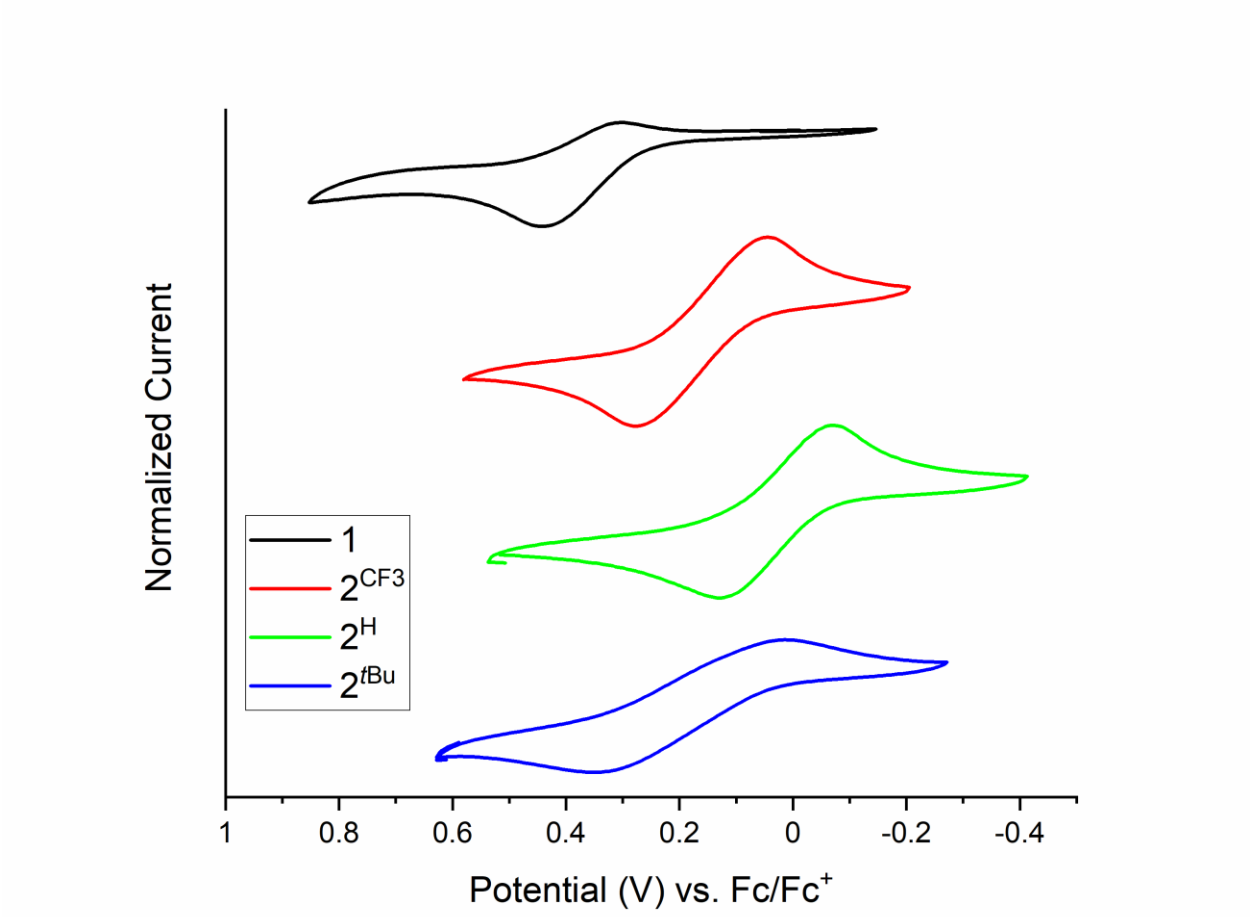

Figure S40. Cyclic Voltammogram (100 mV/s) of **1**, **2^{CF3}**, **2^{H}**, and **2^{tBu}** recorded in CH_2Cl_2 with 0.10 M $[Bu_4N][PF_6]$ at ambient temperature. Note that **2^{H}** is shifted more negative than **2^{CF3}**. We ascribe this discrepancy to reversible binding of MeCN to **2^{H}**. The unit cell of **2^{H}** features three molecules, one of which contains coordinated MeCN. As detailed in solvent-dependent voltammetry experiments, MeCN solvent systematically shifts reduction potentials more negative, consistent with MeCN coordination to Fe. In the case of **2^{H}** obtained in CH_2Cl_2 solvent, we propose that a low concentration of MeCN (from crystallization) results in reversible coordination to Fe, resulting in a time-averaged peak (coordinated MeCN and uncoordinated MeCN) during the voltammetry experiment.

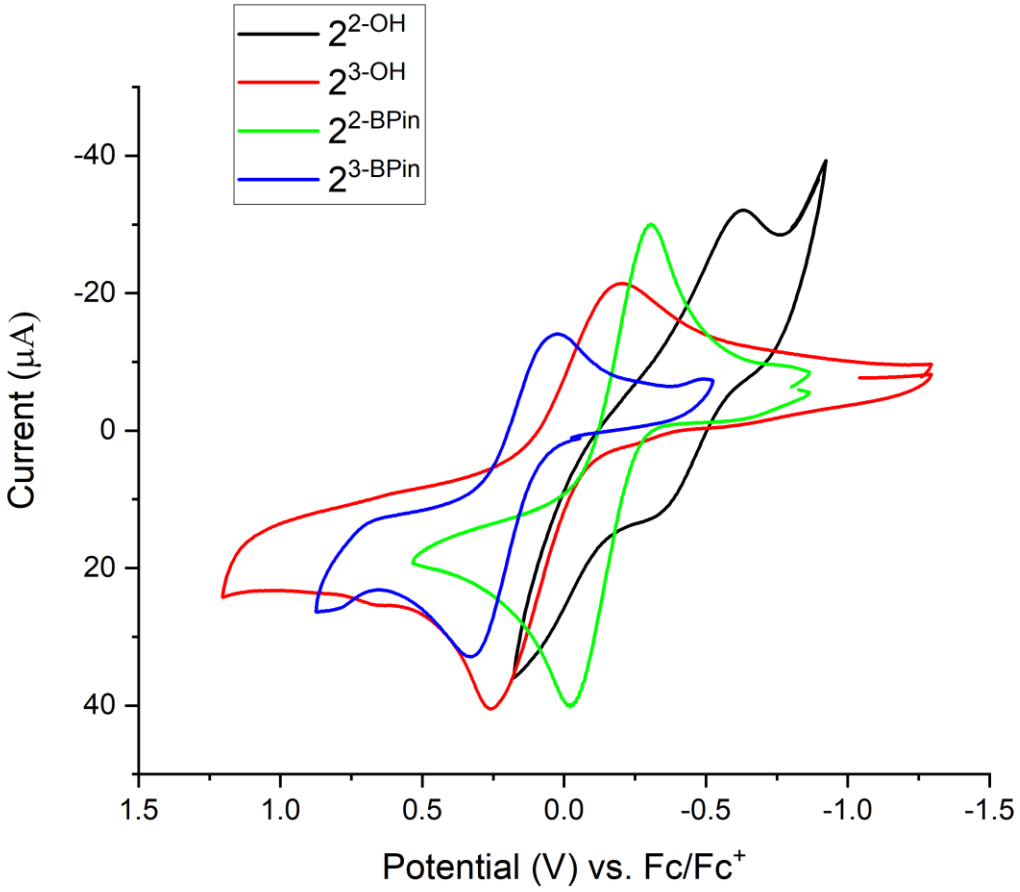

Figure S41. Cyclic Voltammogram (100 mV/s) of $\mathbf{2}^{\mathbf{2\text{-}OH}}$, $\mathbf{2}^{\mathbf{3\text{-}OH}}$, $\mathbf{2}^{\mathbf{2\text{-}BPin}}$ and $\mathbf{2}^{\mathbf{3\text{-}BPin}}$ recorded in CH_2Cl_2 with 0.10 M $[Bu_4N][PF_6]$ at ambient temperature.

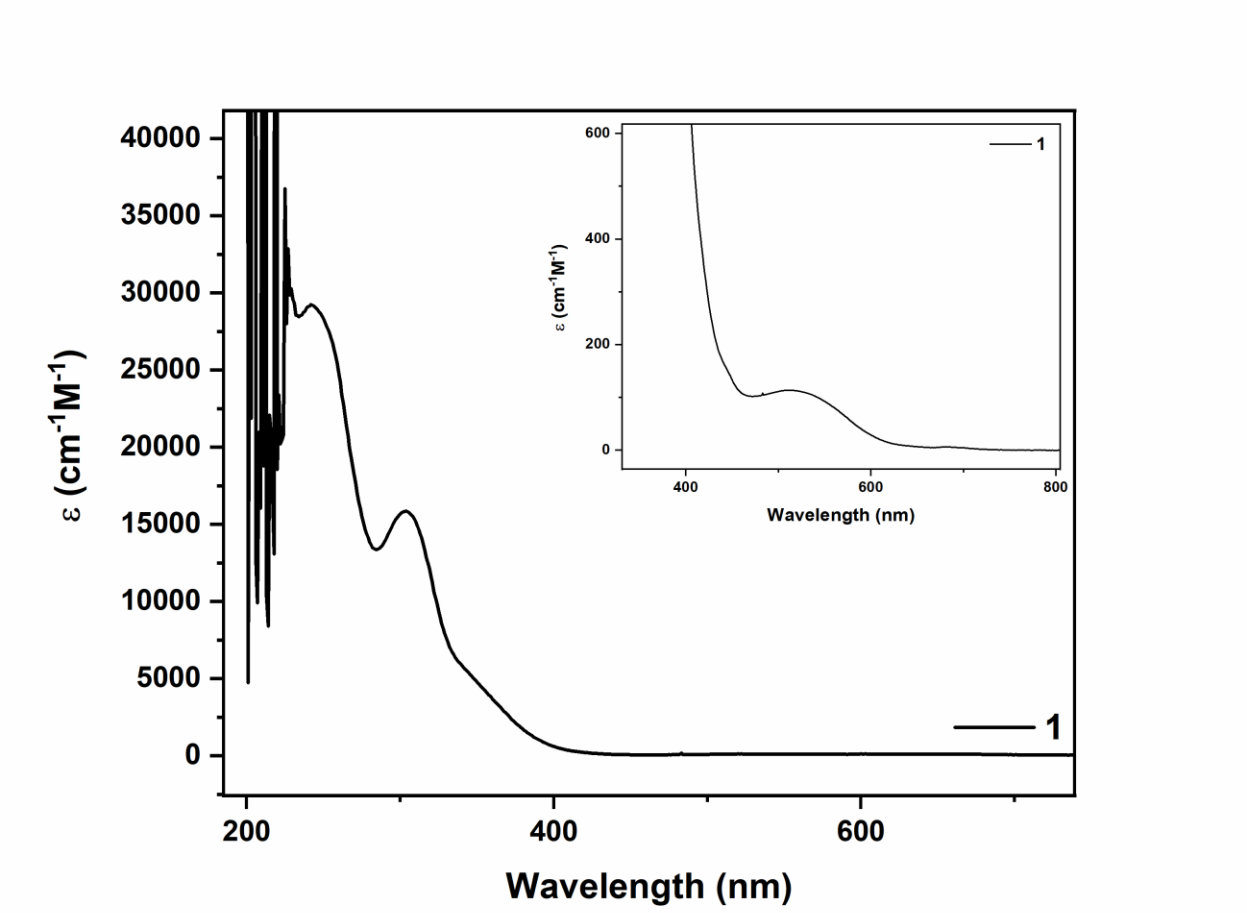

Figure S42. Electronic absorption spectra (CH_2Cl_2, ambient temperature) of **Ph_4P_2-bpyFeCl_2** (**1**).

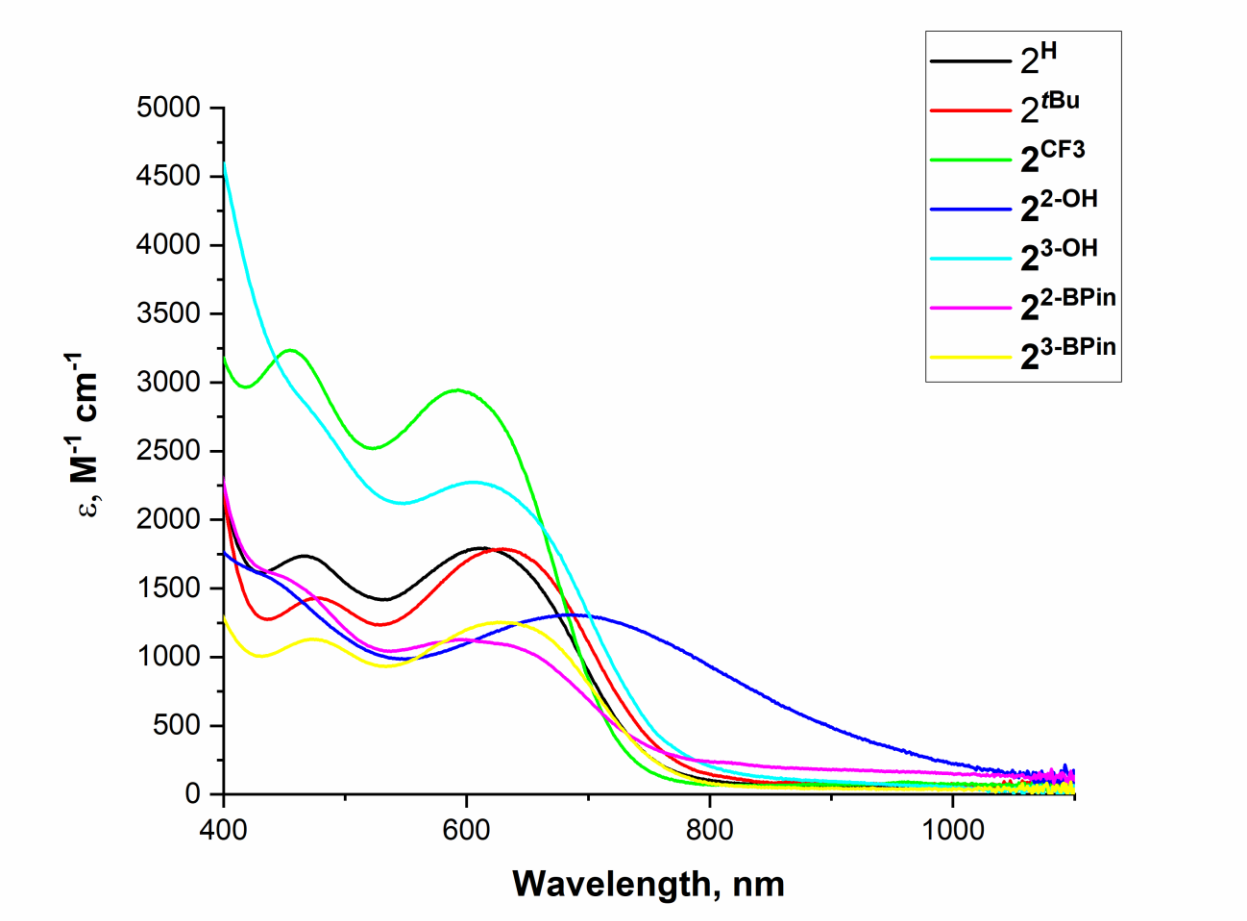

Figure S43. Electronic absorption spectra (CH_2Cl_2, ambient temperature) of **2**^{x}.

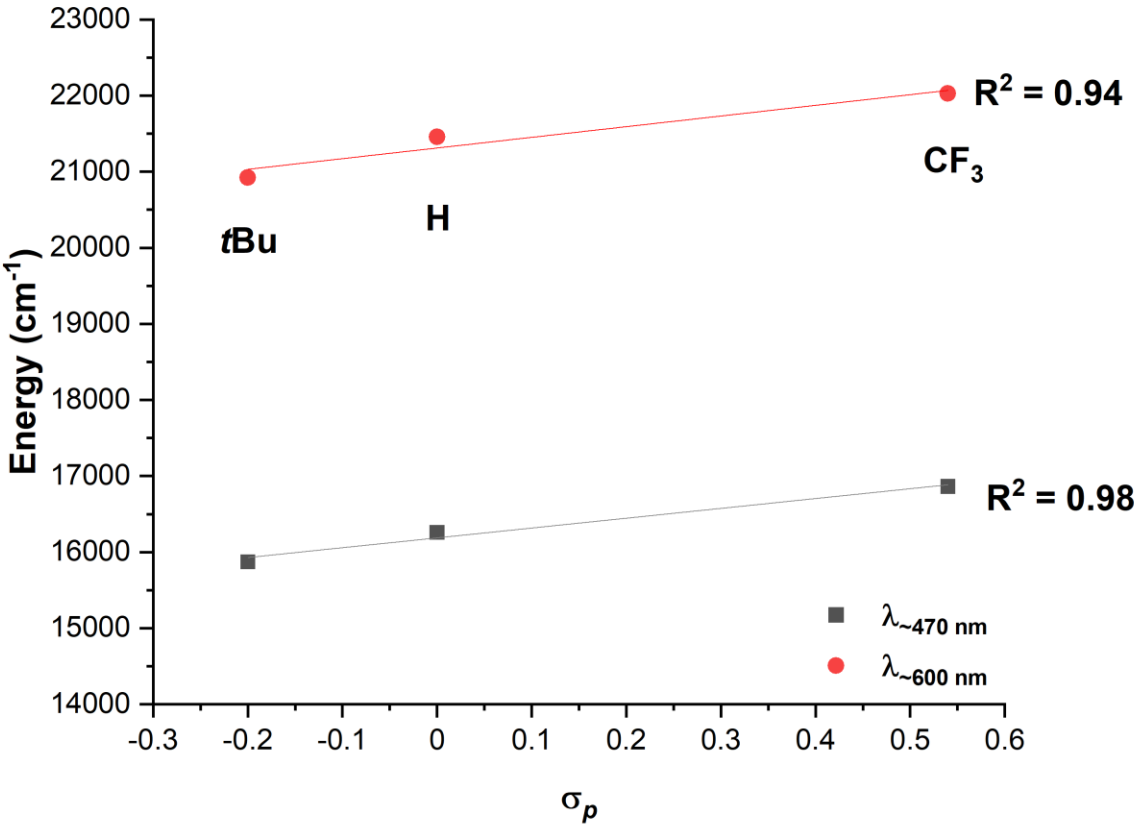

Figure S44. Plot of Hammett parameter (σ_p) vs energy for absorbance bands in UV-vis spectra of $\mathbf{2}^{tBu}$, $\mathbf{2}^{H}$, and $\mathbf{2}^{CF3}$.

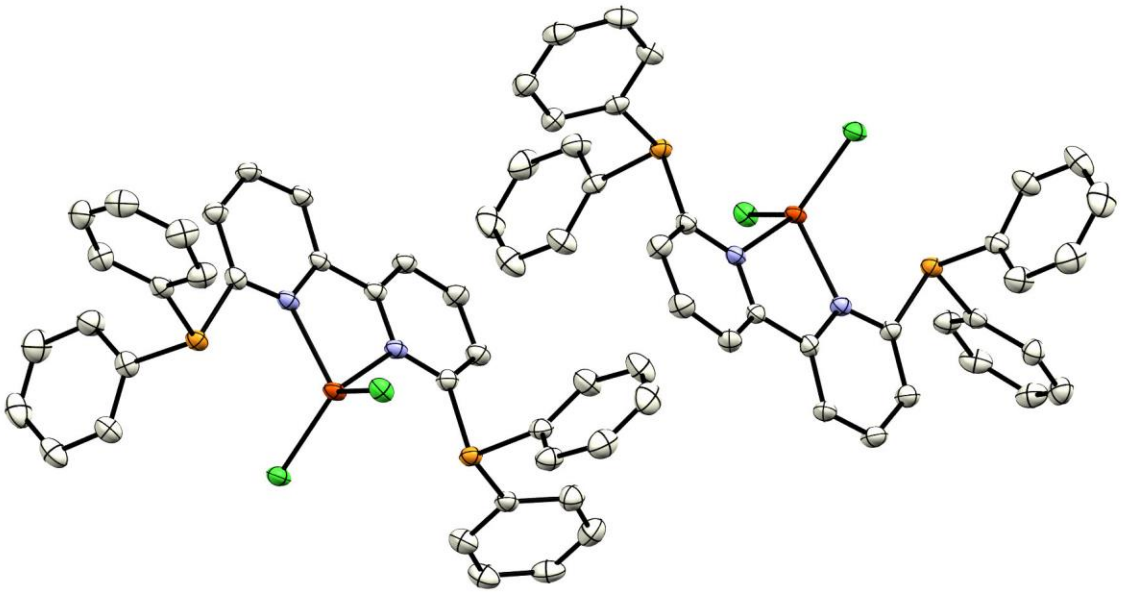

Figure S45. Molecular structures (ORTEP, 50 % probability level) of **1** for the two independent molecules in the unit cell. Hydrogen atoms and solvents have been omitted for clarity.

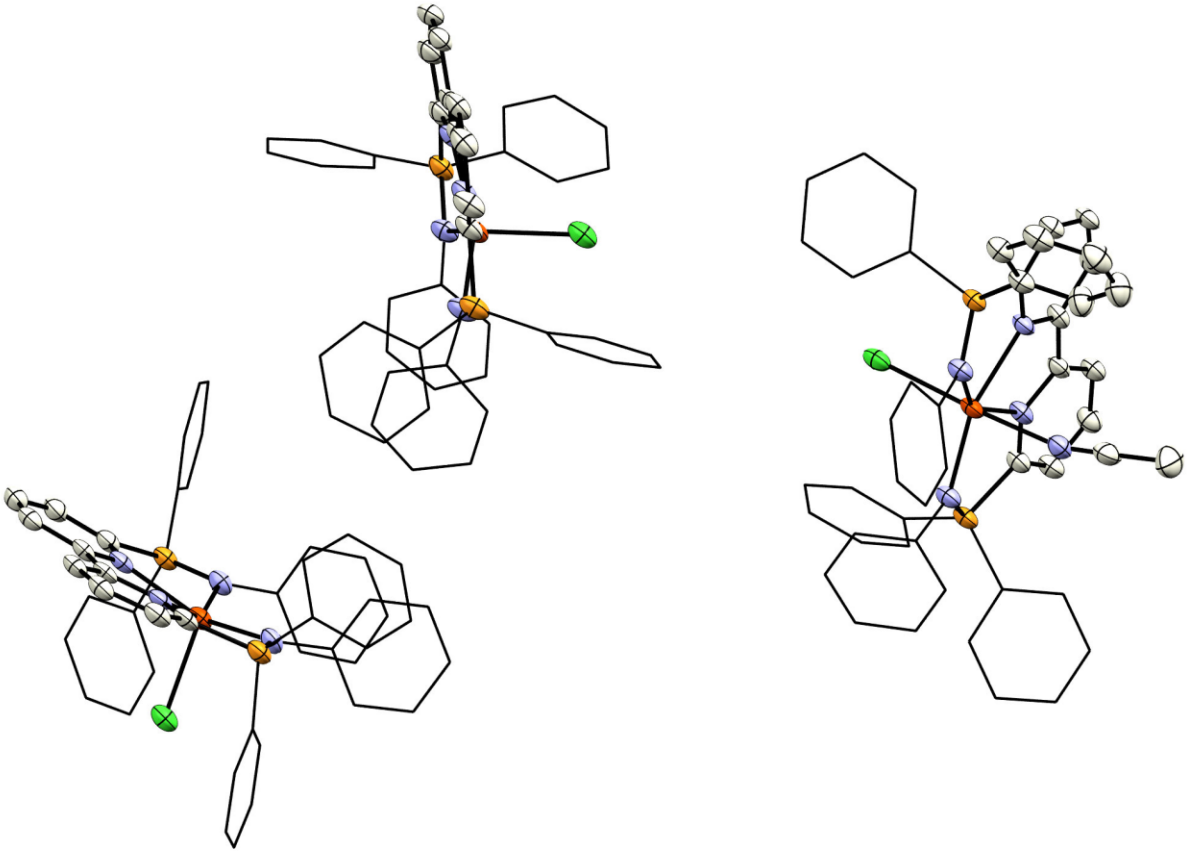

Figure S46. Molecular structures (ORTEP, 50 % probability level) of $\mathbf{2^H}$ for the three independent molecules in the unit cell. Hydrogen atoms, PF_6^- and solvents have been omitted for clarity.

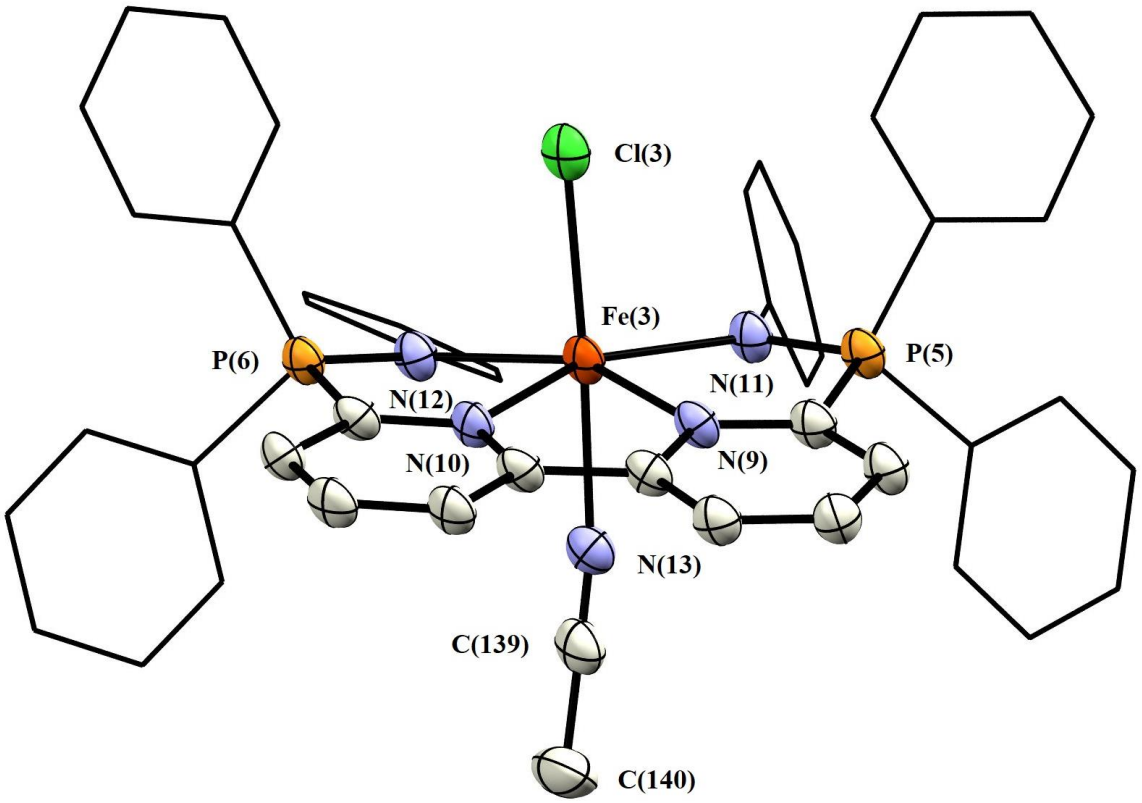

Figure S47. Molecular structures (ORTEP, 50 % probability level) of one of the three crystallographically independent cations of **2^{H}.CH_3CN** coordinated with acetonitrile. Hydrogen atoms and PF_6^- have been omitted for clarity. Selected bond distances (Å) and angles (°) : Fe(3)–N(9) = 2.195(3), Fe(3)–N(10) = 2.187(3), Fe(3)–N(11) = 2.142(3), Fe(3)–N(12) = 2.178(3), Fe(3)–N(13) = 2.285(3), Fe(3)–Cl(3) = 2.5215(8), N(13)–C(139) = 1.118(5), C(139)–C(140) = 1.463(6); N(10)–Fe(3)–N(9) = 72.30(11), N(11)–Fe(3)–N(9) = 79.64(11), N(12)–Fe(3)–N(10) = 79.94(11), N(13) –Fe(3)–Cl(3) = 177.08(8), N(13)–C(139)–C(140) = 179.0(5).

Complex: Ph_4P_2-bpyFeCl_2

Local name: **gr535**

CCDC 2070173

Table S1. Experimental parameters of Ph_2P-bpyFeCl_2.

Crystal data	
Chemical formula	$C_{34}H_{26}Cl_2FeN_2P_2 \cdot C_4H_8O$
M_r	723.36
Crystal system, space group	Monoclinic, *I*2
Temperature (K)	85
a, *b*, *c* (Å)	19.7052 (3), 7.9644 (1), 22.6050 (3)
β (°)	100.994 (1)
V (Å^3)	3482.52 (8)
Z	4
Radiation type	Cu *K*α
μ (mm^{-1})	6.01
Crystal size (mm)	0.12 × 0.12 × 0.06
Data collection	
Diffractometer	Dtrek-*CrysAlis PRO*-abstract goniometer imported rigaku-*D*TREK* images
Absorption correction	Multi-scan *CrysAlis PRO* 1.171.38.41 (Rigaku Oxford Diffraction, 2015) Empirical absorption correction using spherical harmonics, implemented in SCALE3 ABSPACK scaling algorithm.
T_{min}, T_{max}	0.675, 1.000
No. of measured, independent and observed [$I > 2\sigma(I)$] reflections	26906, 6242, 6141
R_{int}	0.041
$(\sin \theta/\lambda)_{max}$ (Å^{-1})	0.606
Refinement	
$R[F^2 > 2\sigma(F^2)]$, $wR(F^2)$, S	0.030, 0.081, 1.03
No. of reflections	6242
No. of parameters	417
No. of restraints	1
H-atom treatment	H-atom parameters constrained
$\Delta\rangle_{max}$, $\Delta\rangle_{min}$ (e Å^{-3})	0.32, -0.35
Absolute structure	Refined as an inversion twin.
Absolute structure parameter	0.499 (5)

Computer programs: *CrysAlis PRO* 1.171.38.41 (Rigaku OD, 2015), *SHELXS97* (Sheldrick, 2008),

SHELXL2018/3 (Sheldrick, 2015, 2018), SHELXLE Rev1005 (Hübschle *et al.*, 2011).

Refinement Details:

Refined as a 2-component inversion twin. Flack parameter 0.499(5).

The structure is pseudo-inversion symmetric emulating space group I2/c. Exact higher symmetry is broken by ordering of the solvate THF molecule.

Complex: **2^{H}**

Local name: **gr569**

CCDC 2070174

Table S2. Experimental parameters of **2^{H}.**

Crystal data	
Chemical formula	$C_{48}H_{39}Br_{0.37}Cl_{0.63}FeN_5P_2 \cdot C_{46}H_{36}Br_{0.27}Cl_{0.73}FeN_4P_2 \cdot C_{46}H_{36}Br_{0.22}Cl_{0.77}FeN_4P_2 \cdot 3(F_6P_3) \cdot 4.38(C_4H_{10}O)$
M_r	3233.35
Crystal system, space group	Triclinic, $P\bar{1}$
Temperature (K)	85
a, *b*, *c* (Å)	15.2634 (3), 20.6508 (4), 24.3094 (3)
α, β, γ (°)	85.532 (1), 81.354 (1), 82.679 (2)
V (Å^3)	7500.0 (2)
Z	2
Radiation type	Cu *K*α
μ (mm^{-1})	4.51
Crystal size (mm)	0.12 × 0.08 × 0.05
Data collection	
Diffractometer	Dtrek-*CrysAlis PRO*-abstract goniometer imported rigaku-*D*TREK* images
Absorption correction	Multi-scan *CrysAlis PRO* 1.171.38.41 (Rigaku Oxford Diffraction, 2015) Empirical absorption correction using spherical harmonics, implemented in SCALE3 ABSPACK scaling algorithm.
T_{min}, T_{max}	0.483, 1.000
No. of measured, independent and observed [$I > 2\sigma(I)$] reflections	115627, 27094, 22290
R_{int}	0.082
$(\sin \theta/\lambda)_{max}$ (Å^{-1})	0.608
Refinement	
$R[F^2 > 2\sigma(F^2)]$, $wR(F^2)$, *S*	0.061, 0.167, 1.02
No. of reflections	27094
No. of parameters	2108
No. of restraints	762
H-atom treatment	H-atom parameters constrained
$\Delta\rangle_{max}$, $\Delta\rangle_{min}$ (e Å^{-3})	0.71, -0.71

Computer programs: *CrysAlis PRO* 1.171.38.41 (Rigaku OD, 2015), *SHELXS97* (Sheldrick, 2008), *SHELXL2018*/3 (Sheldrick, 2015, 2018), SHELXLE Rev1005 (Hübschle *et al.*, 2011).

Refinement Details:

Iron bound chloride atoms are disordered with a small fraction of bromide, and we attribute the bromide to trace contamination. We note that, although this bromide adduct might have higher crystallinity, the overall bromide content is minimal because the bulk material passes CHN combustion analysis (Anal. calcd. for $C_{46}H_{36}ClF_6FeN_4P_3$ (943.03 g/mol): C, 58.59; H, 3.85; N, 5.94. Found C, 58.82; H, 3.90; N, 6.36 %.).

Positions and ADPs of overlapping atoms were constrained to be each identical. Subject to these conditions occupancy ratios refined to to 0.773(4) to 0.227(4) for Cl1/Br1, to 0.726(4) to 0.274(4) for Cl2/Br2, and 0.626(4) to 0.374(4) for Cl3/Br3.

Several solvent occupied pockets were refined as consisting of disordered diethyl ether molecules. All diethyl ether moieties were restrained to have similar geometries. U^{ij} components of ADPs for disordered atoms closer to each other than 2.0 Å were restrained to be similar. Occupancies were constrained to unity where two moieties overlapped. For all other moieties no attempts were made to match occupancies. Subject to these conditions the occupancy rates of the diethyl ether moieties to 0.687(8) (O1), 0.623(5) (O2), 0.639(5) (O3), 0.711(7) (O4), 0.313(8) (O5), 0.377(5) (O6), 0.289(7) (O7), 0.377(5) (O8), and 0.361(5) (O9).

Complex: **2^{tBu}**

Local name: **gr5173**

CCDC 2070171

Table S3. Experimental parameters of **2^{tBu}**.

Crystal data	
Chemical formula	$C_{54}H_{52}ClFeN_4P_2 \cdot F_6P \cdot 1.279(C_4H_{10}O) \cdot 0.666(C_2H_3N)$
M_r	1177.35
Crystal system, space group	Monoclinic, $P2_1/c$
Temperature (K)	85
a, b, c (Å)	19.7512 (2), 18.6528 (1), 17.5182 (2)
β (°)	114.124 (1)
V (Å^3)	5890.30 (10)
Z	4
Radiation type	Cu $K\alpha$
μ (mm^{-1})	3.77
Crystal size (mm)	0.12 × 0.10 × 0.05
Data collection	
Diffractometer	Dtrek-*CrysAlis PRO*-abstract goniometer imported rigaku-*D*TREK* images
Absorption correction	Multi-scan *CrysAlis PRO* 1.171.38.41 (Rigaku Oxford Diffraction, 2015) Empirical absorption correction using spherical harmonics, implemented in SCALE3 ABSPACK scaling algorithm.
T_{min}, T_{max}	0.543, 1.000
No. of measured, independent and observed [$I > 2\sigma(I)$] reflections	89910, 10934, 10490
R_{int}	0.050
$(\sin \theta/\lambda)_{max}$ (Å^{-1})	0.607
Refinement	
$R[F^2 > 2\sigma(F^2)]$, $wR(F^2)$, S	0.041, 0.112, 1.06
No. of reflections	10934
No. of parameters	989
No. of restraints	1015
H-atom treatment	H-atom parameters constrained
$\Delta\rangle_{max}$, $\Delta\rangle_{min}$ (e Å^{-3})	0.69, -0.34

Computer programs: *CrysAlis PRO* 1.171.38.41 (Rigaku OD, 2015), *SHELXS97* (Sheldrick, 2008), *SHELXL2018*/3 (Sheldrick, 2015, 2018), SHELXLE Rev1005 (Hübschle *et al.*, 2011).

A p-^{t}Bu-phenylene group was refined as disordered by a rotation of the ^{t}Bu group that induced a deflection of the phenylene ring. The two disordered moieties were restrained to have similar geometries as another not disordered p-^{t}Bu-phenylene group. U^{ij} components of ADPs for disordered atoms closer to each other than 2.0 Å were restrained to be similar. Subject to these conditions the occupancy ratio refined to 0.633(6) to 0.367(6).

A solvent occupied pocket was refined as consisting of disordered acetonitrile and diethyl ether molecules. The acetonitrile moiety was refined without restraints for atom positions. All diethyl ether moieties were restrained to have similar geometries. U^{ij} components of ADPs for disordered atoms closer to each other than 2.0 Å were restrained to be similar. Occupancies were constrained to unity where two moieties overlapped. For all other moieties no attempts were made to match occupancies. Subject to these conditions the occupancy rate of the acetonitrile molecule refined to 0.633(6) to 0.666(6). Those of the diethyl ether moieties to 0.334(6) (O1), 0.317(5) (O2), 0.086(4) (O3), 0.360(5) (O4) and 0.182(5) (O5).

Complex: **2^{CF3}**

Local name: **gr5174**

CCDC 2070172

Table S4. Experimental parameters of **2^{CF3}.**

Crystal data	
Chemical formula	$C_{48}H_{34}ClF_6FeN_4P_2 \cdot F_6P \cdot 1.155(C_4H_{10}O) \cdot 0.734(C_2H_3N)$
M_r	1194.74
Crystal system, space group	Monoclinic, $P2_1/c$
Temperature (K)	85
a, b, c (Å)	18.0420 (2), 18.7721 (2), 17.1927 (2)
β (°)	112.116 (1)
V (Å^3)	5394.50 (11)
Z	4
Radiation type	Cu $K\alpha$
μ (mm^{-1})	4.30
Crystal size (mm)	0.13 × 0.11 × 0.09
Data collection	
Diffractometer	Dtrek-*CrysAlis PRO*-abstract goniometer imported rigaku-*D*TREK* images
Absorption correction	Multi-scan *CrysAlis PRO* 1.171.38.41 (Rigaku Oxford Diffraction, 2015) Empirical absorption correction using spherical harmonics, implemented in SCALE3 ABSPACK scaling algorithm.
T_{min}, T_{max}	0.637, 1.000
No. of measured, independent and observed [$I > 2\sigma(I)$] reflections	81879, 10032, 9083
R_{int}	0.060
$(\sin \theta/\lambda)_{max}$ (Å^{-1})	0.607
Refinement	
$R[F^2 > 2\sigma(F^2)]$, $wR(F^2)$, S	0.044, 0.124, 1.06
No. of reflections	10032
No. of parameters	851
No. of restraints	427
H-atom treatment	H-atom parameters constrained
$\Delta\rangle_{max}$, $\Delta\rangle_{min}$ (e Å^{-3})	0.39, -0.69

Computer programs: *CrysAlis PRO* 1.171.38.41 (Rigaku OD, 2015), *SHELXS97* (Sheldrick, 2008), *SHELXL2018*/3 (Sheldrick, 2015, 2018), SHELXLE Rev1005 (Hübschle *et al.*, 2011).

Refinement Details:

A CF_3 group was refined as disordered by rotation. The two disordered moieties were restrained to have similar geometries as another not disordered CF_3 group. U^{ij} components of ADPs for disordered atoms closer to each other than 2.0 Å were restrained to be similar. Subject to these conditions the occupancy ratio refined to 0.464(11) to 0.536(11).

A solvent occupied pocket was refined as consisting of disordered acetonitrile and diethyl ether molecules. The two acetonitrile moieties were to have similar geometries, and the C-C bond of the pivot moiety was restrained to a length of 1.51(2) Å. All diethyl ether moieties were restrained to have similar geometries. U^{ij} components of ADPs for disordered atoms closer to each other than 2.0 Å were restrained to be similar. Occupancies were in part constrained to unity where two moieties overlapped, but no attempts were made to match all occupancies. Subject to these conditions the occupancy rates of the acetonitrile molecules refined to 0.573(3) and 0.161(6). Those of the diethyl ether moieties to 0.728(2) (O1), 0.272(2) (O2) and 0.155(2) (O3).

Complex: **$2^{3\text{-BPin}}$**

Local name: **DeebTaher115_0m**

CCDC 2070170

Table S5. Experimental parameters of **$2^{3\text{-BPin}}$**.

Crystal data	
Chemical formula	$C_{58}H_{58}B_2ClFeN_4O_4P_2 \cdot F_6P \cdot 1.397(C_4H_{10}O) \cdot 0.74(CH_2Cl_2)$
M_r	1361.28
Crystal system, space group	Monoclinic, $P2_1/c$
Temperature (K)	150
a, b, c (Å)	23.1444 (16), 18.7701 (9), 17.1873 (8)
β (°)	110.277 (2)
V (Å^3)	7003.8 (7)
Z	4
Radiation type	Mo $K\alpha$
μ (mm^{-1})	0.44
Crystal size (mm)	0.35 × 0.32 × 0.05
Data collection	
Diffractometer	Bruker AXS D8 Quest diffractometer with PhotonII charge-integrating pixel array detector (CPAD)
Absorption correction	Multi-scan *SADABS* 2016/2: Krause, L., Herbst-Irmer, R., Sheldrick G.M. & Stalke D. (2015). J. Appl. Cryst. 48, 3-10.
T_{min}, T_{max}	0.633, 0.746
No. of measured, independent and observed [$I > 2\sigma(I)$] reflections	114702, 21068, 12382
R_{int}	0.113
$(\sin \theta/\lambda)_{max}$ (Å^{-1})	0.716
Refinement	
$R[F^2 > 2\sigma(F^2)]$, $wR(F^2)$, S	0.067, 0.220, 1.02
No. of reflections	21068
No. of parameters	1152
No. of restraints	1146
H-atom treatment	H-atom parameters constrained
$\Delta\rangle_{max}$, $\Delta\rangle_{min}$ (e Å^{-3})	1.15, -0.63

Computer programs: Apex3 v2019.1-0 (Bruker, 2019), *SAINT* V8.40A (Bruker, 2019), *SHELXS97* (Sheldrick, 2008), *SHELXL2018*/3 (Sheldrick, 2015, 2018), SHELXLE Rev1117 (Hübschle *et al.*, 2011).

Refinement Details:

The two dioxaborolane substituents are disordered by inflection of the ethylene groups. Major and minor disordered moieties were restrained to have similar geometries. U^{ij} components of ADPs for disordered atoms closer to each other than 2.0 Å were restrained to be similar. Subject to these conditions the occupancy ratio refined to 0.684(6) to 0.684(6) for the moieties of B1, and to 0.408(9) to 0.592(9) for the moiety of B2.

A solvate pocket is occupied by extensively disordered diethyl ether and methylene chloride molecules. C-Cl bond lengths were restrained to a target value of 1.70(2) Å. All ether moieties were restrained to have similar geometries, and ether C-C bonds were restrained to a target value of 1.53(2) Å. U^{ij} components of ADPs for disordered atoms closer to each other than 2.0 Å were restrained to be similar. Occupancies for disordered solvate molecules were freely refined. Subject to these conditions occupancy rates refined to 0.589(5) and 0.151(8) for the two methylene chloride moieties, and to 0.368(12), 0.226(10), 0.335(7), 0.362(10) and 0.106(7).

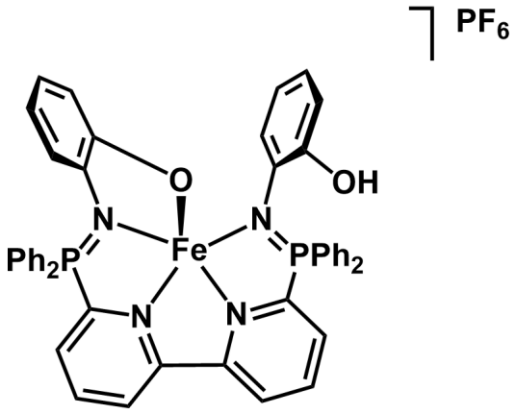

Figure S48. Proposed solution structure of $\mathbf{2}^{\mathbf{2\text{-}OH}}$.

References

[1] K. Barral, A. D. Moorhouse, and J. E. Moses Org. Lett. 2007, 9, 1809-1811.

[2] D. Xin, A. Qin, B. Z. Tang Polym. Chem. 2019, 10, 4271–4278.

[3] C. Zanato, M. G. Cascio, P. Lazzari, R. Pertwee, A. Testa, M. Zanda, Matteo, Synthesis 2015, 47, 817–826.

[4] A. T. Tran, K. M. Cergol, W. J. Britton, S. A Imran Bokhari, M. Ibrahim, A. J. Lapthorn, R. J. Payne MedChemComm 2010, 1, 271–275.

[5] J. E. M. Lewis, F. Modicom, S. M. Goldup, Stephen M. J. Am. Chem. Soc. 2018, 140, 4787–4791.

[6] C. Kong, N. Jana, C. Jones and T. G. Driver, J. Am. Chem. Soc. 2016, 138, 13271–13280.

[7] I. G. Powers, J. M. Andjaba, X. Luo, J. Mei, C. Uyeda J. Am. Chem. Soc. 2018, 140, 4110–4118.

[8] Y. Uchida and N. Echikawa Heteroat. Chem. 1994, 5, 904-912.

[9] R. Ziessel Tetrahedron Lett. 1989, 30, 463-466.

[10] Rigaku Corp., The Woodlands, Texas, USA.

[11] Otwinowski Z, Minor W., Processing of X-ray diffraction data collected in oscillation mode. Methods Enzymol. 1997, 276, 307–326.

[12] L. Krause, R. Herbst-Irmer, G.M. Sheldrick and D. Stalke J. Appl. Cryst. 2015, 48, 3-10.

[13] P. van der Sluis, A. L. Spek Acta Crystallogr., Sect. A. 1990, 46, 194–201.

[14] Bruker Advanced X-ray Solutions, Saint v8.34A, (2014).

[15] G. M. Sheldrick Acta Crystallogr., Sect. A. 2008, 64, 112–122.